The Relationship Between Lattice Structure Topology and Rapid Investment Casting Performance

Christopher Richard

A Thesis
in
The Department
of
Mechanical Engineering

Presented in Partial Fulfillment of the Requirements
for the Degree of Master of Applied Sciences (Mechanical Engineering) at
Concordia University
Montreal, Quebec, Canada

September 2020

CONCORDIA UNIVERSITY

School of Graduate Studies

This is to certify that the thesis prepared

By: Christopher Richard

Entitled: *The Relationship Between Lattice Structure Topology and Rapid Investment Casting Performance*

and submitted in partial fulfillment of the requirements for the degree of

Master of Applied Sciences (Mechanical Engineering)

complies with the regulations of the University and meets the accepted standards with respect to originality and quality.
Signed by the Final Examining Committee:

Dr. Martin Pugh Chair
Chair's name

Dr. Zezhong Chen Examiner
Examiner's name

Dr. Tsz-Ho Kwok Supervisor
Supervisor's name

Approved by: Dr. Sivakumar Naranswamy
Chair of Department or Graduate Program Director

September 16th 2019 Dr. Mourad Debbabi
Dean of Faculty

Abstract

The Relationship Between Lattice Structure Topology and Rapid Investment Casting Performance

Christopher Richard

To leverage the unprecedented design freedom of additive manufacturing (AM), this work aims to develop a design methodology for lattice structures fabricated by rapid investment casting (RIC). What lattice topological properties have the most significant impact on the overall performance in RIC, and how to improve them? The hypothesis is that the relative strut size, number of joints, joint valence, and strut angle significantly affect the performance. There is no overarching analysis of the effect that lattice topology has on casting performance. To remedy this, various lattice topologies underwent mold flow simulation, finite element analysis, casting experiments, and grain structure analysis. From the results, a set of design guidelines for RIC is created, and new lattice structures are designed. The design recommendations by importance are as follows. A relative strut size, number of joints, and joint valence should be below 0.20, 9, and 8, respectively. For mechanical performance, the strut angle distribution should include vertical, diagonal, and horizontal struts. The two proposed topologies: proposed cell and hourglass, meet all these criteria and achieve good casting and mechanical performance.

Acknowledgements

I would like to acknowledge everyone who helped me during my degree. My parents and friends for their unconditional support. I would like to thank the Birks Family Foundation for there support throughout the entirety of my education with special regards to Mr. J. Birks and Mrs. G. Carozza.

I would like to thank my supervisor Tsz-Ho Kwok for his incredible support, ensuring I have all the equipment necessary to complete my Master's and his encouragement and tutelage.

Contents

List of Figures

List of Tables

Chapter 1

Introduction

Currently, the most studied metal AM process is SLM. SLM has many positive aspects, which make it a topic of interest, but also some limitations. According to Aboulkair et al. [5], one of the most common defects in SLM parts in general, irrespective of the material, is porosity. Maconachie et al. [6] also mentioned that SLM fabrication of lattice structures is understood to result in manufacturing defects. Beyond that metallic additive manufacturing methods cannot be used for mass manufacturing of complex parts. This is due to the high cost associated with the process. Alternatively multiple patterns for RIC can be made at a very low cost and depending on the geometry can be made hollow to save on material usage and print time. According to Leuders et al. [7], When comparing RIC to SLM, fatigue loadings are still a challenge for SLM, and the same is true for selective sintering (SLS). Li et al. [8] demonstrated the presence of residual stresses in most metal AM processes. The residual stresses are due to high temperature gradient and rapid cooling. Given that RIC is a hybrid AM and solidification process, it is less prone to residual stresses. In addition of the three manufacturing processes, investment casting (IC) is already well established in many industries that would benefit from a shift towards RIC. RIC has similar capabilities as SLM. Both methods have their respective uses and place in the additive manufacturing space, but RIC performs better in some applications. One example is in the manufacturing of aluminum alloy structures, which is a challenge for SLM to process because aluminum is reflective, and the laser has difficulties melting aluminum without causing defects [5]. Also, RIC

does not require sintering, which often leads to considerable shrinkage. The use of SLM for lightweight cellular structures has been heavily iterated and researched. The result is a vast trove of knowledge regarding materials, parameters, and design methodologies for metallic additive manufacturing of cellular lattice structures. Although RIC can also be used to manufacture complex lattice structures with unprecedented design freedom, little work has been done to advance the design methodology for RIC of lattice structures. The limited research includes using fused filament fabrication (FFF) to produce low-cost patterns [9], studying the effect of cross-sectional shape of struts on mechanical properties [10], and finding the optimal filling direction for honeycomb structures [11]. However, there is no current overarching analysis of the effect that lattice topology has on casting performance and what topological properties play the most extensive role in minimizing casting defects. Lattice topology is defined as the properties of a lattice structure in 3D that remain the same regardless of deformations such as twisting and stretching. For strut-based lattice topologies these properties are the bounding volume, unit cell density, and strut shape/distribution/connectivity. This analysis is required to avoid casting defects in lattice structures to faithfully apply them to metal parts. There are many benefits to RIC over other manufacturing processes. RIC can produce parts with complex geometries such as: thin sections, cavities and complex internal lattice structures. Beyond that, RIC requires very little post processing and it can produce parts with great dimensional accuracy and surface finish. Finally, RIC components do not suffer from poor fatigue strength so it can be used in industries like aerospace, dentistry and biomedical engineering, etc. This work will present the background information on IC and RIC and then delve deeper into the current open areas of research. Some areas of research show more potential towards improving the manufacturing process as a whole and these will be presented with the intention of identifying the most lucrative research directions in RIC.

Given that RIC is a hybrid manufacturing method with both additive and solidification processes, its design considerations stem from both methods. To

correctly print the pattern, design for AM needs to be applied. Considerations include print direction, support location, and overhang angle. The AM performance depends heavily on the chosen AM method, the topology of the pattern and supports, and the material and process parameters. Some common pattern making methods are: fused filament fabrication (FFF), stereolithography apparatus (SLA), digital light processing (DLP) and Multi-Jet Modeling (MJM) see Fig 1.1.

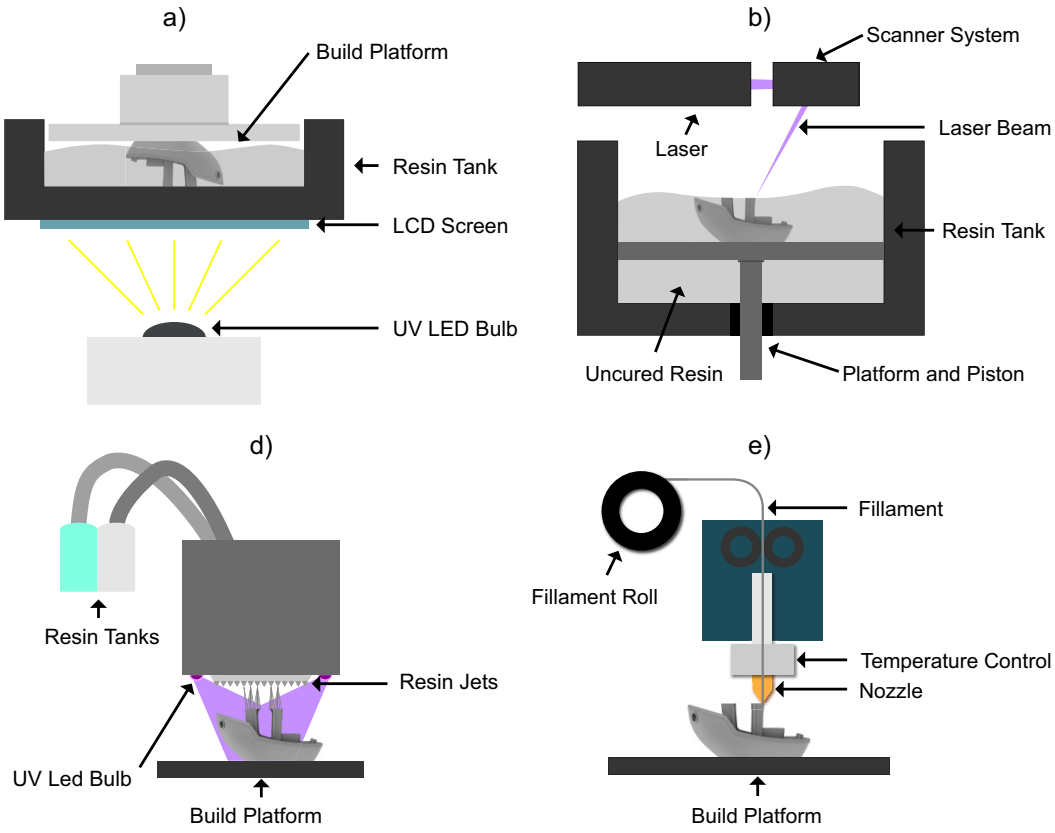

FIGURE 1.1: Pattern Making AM Processes: a)Digital Light Processing. b) Stereolithography Apparatus. c) Multi-Jet Modeling. d) Fused Filament Fabrication.

FFF is a 3D printing process in which plastic filament made from PLA (polylactic acid), ABS (acrylonitrile butadiene styrene) etc. is melted through a heated nozzle and deposited following a tool path on a print bed. Tool paths can be generated using a slicer software. The software breaks down 3D models into layers each with its own tool path. SLA and DLP are photo-curable resin based processes, SLA uses a laser to cure a layer point by point and layer by layer. DLP uses a projector or LCD to cure full layers at a time. The

benefits of these 3D printing processes are that they can create really high quality patterns with great surface finishes. The RIC process can be seen in Fig 1.2. Conventional manufacturing methods impose geometric restrictions this is not the case for RIC. IC uses a sacrificial pattern to form a mold. This is done by encasing the pattern in refractory material. The pattern then undergoes a burnout process leaving a mold cavity in the shape of the pattern. Molten metal can then be poured into the mold cavity creating a metal part with the same geometry as the pattern. Design for IC has its own set of considerations: feeding direction, gating and feeding system design, and pattern topology. The IC performance depends heavily on the pattern and gating system topology and its inherent mold flow. Like many processes, topology optimization can be applied to casting. Topology optimization for casting relies primarily on the following properties: feed paths, flow velocity and flow connectivity. Feed paths are used to ensure directional solidification moving from thin to thick. Risers can be placed to allow for directional solidification that sweeps from the extremities of the mold cavity toward the riser. Flow velocity can be optimized to ensure molten metal does not prematurely solidify. Finally flow connectivity can be controlled to avoid turbulence or hot spots. Minimizing the number of intersections of metal flows will allow the casting to cool at similar rates throughout, this will avoid the potential for hot spots which result in localized shrinkage voids. Studying the effect of lattice topology on RIC performance will help draw out the optimization objectives in order to be able to eventually apply topology optimization to the casting of lattice structures. When it comes to the design of lattice structures for RIC, the lattice topology is one of the most critical factors that affects printability, castability, and mechanical properties. Different objectives may have contradicting requirements on the topology, and the research question here is: what lattice topological properties have the most significant impact on the overall performance in RIC, and how to improve them? In this work, a few properties are hypothesized, including the relative strut size, number of joints, joint valence, and strut angle, significantly affect the casting performance. These properties can be evaluated using a variety of lattice

topologies and structures. The relative strut size is the strut size divided by the unit cell width, which is a property that will remain the same regardless of unit cell width. The number of joints refers to the total number of points within the cell where struts connect. Joint valence refers to how many struts connect at a given joint. Strut length is the distance traveled by the metal flow in the lattice cell. Strut angle is the angle of the strut from the filling direction of the lattice structure. These properties were chosen as they relate to the definition of lattice topology. Relative strut size and strut shape directly affect unit cell density. Number of joints, joint valence and strut angle directly affect strut distribution/connectivity.

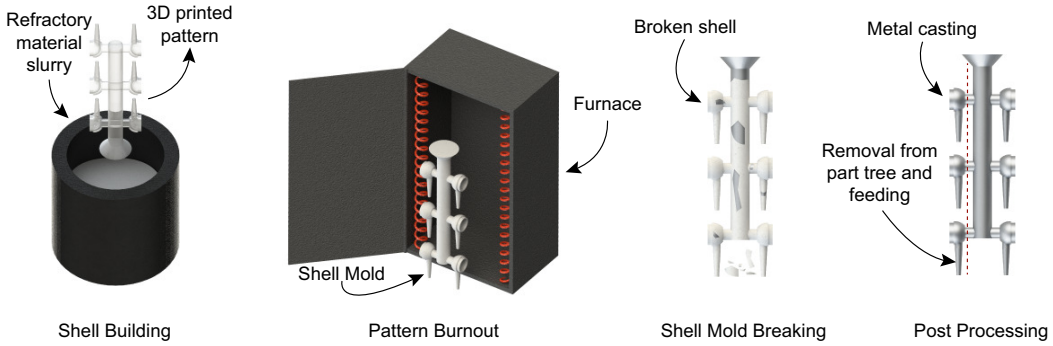

FIGURE 1.2: Rapid Investment Casting Process

By answering the research question, this work aims to develop a design methodology for RIC lattice structures. The goal of the design methodology would be to minimize casting defects caused by the lattice topology. Since RIC's design is a multi-objective optimization, only the lattice structures with excellent printability are selected, i.e., self-supported and open-celled, and focus on improving the castability without sacrificing mechanical performance. These lattices will undergo mold flow and mechanical simulation to determine what defects will occur and which properties are more critical. The casting results will be evaluated and compared with the theoretical results to establish design guidelines for RIC lattice structures. These design guidelines will be used to propose new designs optimized for casting performance. Finally, a larger scale sample of the best performing design will undergo microscopic void and grain structure analysis to verify the simulation results further. The objective of this

work is to expand the limited research on lattice design for RIC as there is no overarching analysis on the effect of lattice topology on casting performance. The contributions of this work include:

- A methodology to study rapid RIC lattice structures' performance is presented to test our hypothesis on the lattice topological properties.
- The properties are compared and analyzed with the test results, and a set of design guidelines for RIC is created.
- Based on the analysis, new lattice structures are designed and optimized for RIC.

This work is organized as follows. Chapter 2 briefly reviews the related works. Chapter 3 details the equipment, materials and methodology used. Chapter 4 describes the theoretical and experimental results of the study. Chapter 5 evaluates the results and establishes an order of importance to the topological lattice properties for casting performance. Finally, the work concludes in Chapter 6.

Chapter 2

Related Work

2.1 Casting Technology

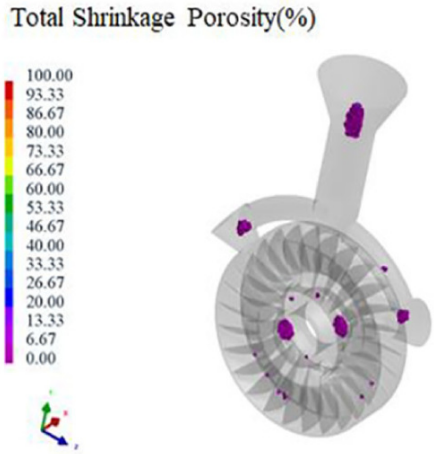

FIGURE 2.1: Casting defects located in cast part. Reprinted by permission from Springer Nature [1] © 2020.

IC was described as taking advantage of a fluid's ability to assume the shape of its container [12]. IC is a extensively developed and refined process. IC was primarily used with precious metals for ornamentation and religious purposes. After 1897, dentists began using the manufacturing processes to make dental inlays. During WWII, IC became the manufacturing process of choice for military aerospace components. Afterwards, the IC process transitioned to many commercial and industrial applications. The applications of IC have evolved from ornamentation to dental and finally aerospace, all these applications are still in use today in addition to biomedical engineering. The main difference with the modern applications is that they test the limits of the process using

complex design elements such as small cross sections and high dimensional accuracy [13]. Given the nature of the process, IC design is principal to good mold flow [1, 14–17]. Poor gating system design could lead to casting defects, this behaviour can be seen in Fig. 2.1. During the optimization of casting homogeneity, the gating system's quality can be the most important factor affecting casting defects occurrence [18]. One way to improve casting performance is using a novel parabolic conical-helical sprue which reduces surface turbulence in metal below critical velocity during mold filling [19]. Poor gating system design could also lead to rough surface finish and accuracy, and a design where the size of sprue and runner is unbalanced will produce unstable molten metal flow [16].

Current research is focused mainly on iterating gating system design optimization in the hopes of reducing the likelihood of casting defects. Gating system design remains an iterative laborious process. There exist design guidelines for the process, but limited research on applying computational methods to automate the process. One exception is the use of computing and data-driven methods for gating and feeding system design in IC. Yu et al. present a data-driven framework coupled with the RBF optimization method for gating system design. The results of the optimization can be seen in Fig 2.2, it can be observed that all the defects occur in the feeders and not the cast part.

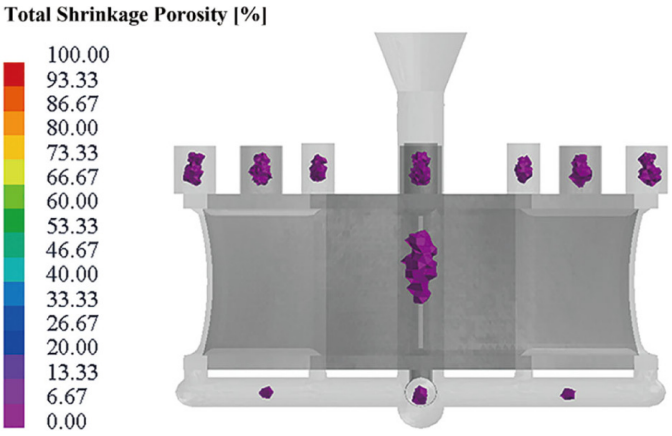

FIGURE 2.2: Numerical simulation and correlation with macro-structure evaluation of the primarily proposed design. Reprinted by permission from Springer Nature [2] © 2020

From the optimizations the gating system's diameter was found to be the most influential on the volume of average shrinkage porosity [2]. This knowledge

can be added to the ever growing design methodology for IC. Conventional IC relies primitive technologies for pattern making but AM is the most popular option to replace the wax used in pattern making [20]. The only difference between IC and RIC is the pattern making method, RIC relies on AM for pattern making. This allows for RIC to take advantage of the full design freedom of AM as it does not need to worry about pattern removal from the mold like its wax alternatives. Let it be noted that for traditional IC the wax pattern is melted whereas for RIC the resin pattern is burned for removal. This means that the wax in IC can be reused to a certain extent, this is not the case for RIC resin. There also exist wax 3D printing processes that can be used for RIC, these processes are a bit slower and the patterns are more delicate than resin for the molding process. For the 3D printed wax, the wax could not directly be reused, it would have to be reprocessed for the 3D printer.

2.2 Additive Manufacturing

Design for IC and AM can be combined to cast a structurally optimized metal components [21] such as the one in Fig 2.3. There exist many AM methods but only several of them are used for pattern and mold making. The RIC processes, mainly using SLA can be found in a review [22]. Given that the dimensional accuracy of the component cast using RIC is highly pattern dependent [23, 24]. Ishida et al. [25] tested the ability of different manufacturing methods to create dimensionally accurate full dental crowns, and they showed that all the methods had their respective drawbacks. Monzon et al. [26] discovered the presence of anisotropy in patterns made using DLP. The authors found that post curing does remove the anisotropy for certain resins where UV light can pass through the resin and pigment. This could be concerning depending on the application for these 3D printed parts. Anisotropy can often associated with nonuniform strength. Even in RIC, anisotropy could cause unpredictable mold cracking. SLA was used by Huang and Huang [27] to compare RIC and traditional IC by creating a miniature turbine blade. They found that SLA can create high

precision casting patterns. MJM can also 3D print using photo-curable resins, but has the benefit of printing in wax materials as well, it can also create much larger parts, with resolutions slightly higher than SLA and DLP. The resolution of 3D prints are highly dependent on the machine and materials used. FDM can be used create much larger parts than its resin based alternatives. Given the low cost and large build volumes, a lot of research has been done to improve its surface finishes and dimensional accuracy. Kumar et al. [28] attempted to improve the surface finish of 3D printed patterns by observing the effect of varying process parameters such as: geometric volume to area ratios, wax coated or uncoated patterns, orientation, mold thickness and material grade in order to achieve high dimensional accuracy when casting a hip joint. They concluded, a thin coating of wax increases accuracy of the patterns being made. Higher volume to area ratios and pattern orientations of 90 degrees lead to higher accuracy. They were able to achieve the permissible tolerances grades determined by the ISO standard. Hafsa [29] and Ibrahim et al. [30] compared the use of two AM methods, MJM and FFF for creating RIC patterns. The authors found that utilizing different internal structure for their patterns had an effect on surface roughness. The main drawback of using FFF for IC is that much effort is required to improve the quality of the printed patterns. Presently FFF can not achieve the quality of patterns that DLP, SLA and MJM can. For small scale IC, given the low cost, high speed and resolution of DLP, it is a excellent choice for pattern making. For larger parts MJM seems to be the best process available at the moment [13].

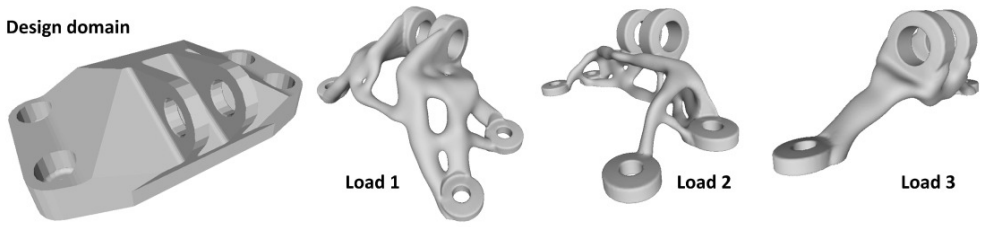

FIGURE 2.3: Topology optimization of the GE bracket for multiple load cases. Reprinted by permission from Springer Nature [3] © 2020

An alternative mold making technique is patternless mold making. This process can improve time efficiency when compared to pattern dependent methods. The burnout process can be omitted for patternless mold making. The main drawback of the process is that it is dependent on SLS or binder jetting technology. The two powder based process both undergo large amounts of shrinkage during the mold sintering processes. The sintering process is required to fully consolidate the ceramic or plaster refractory powders used. Generally the powder based AM processes can produce surface finishes on par with sand casting. This pales in comparison to the surface finish achievable with a pattern. The use of ZCast binder jetting technology has been evaluated to create aluminum castings by reducing the mold wall thickness from 12mm to 5mm. The criteria were dimensional accuracy and surface roughness and were found to be in the range of sand casting [31]. Binder jetting technology has been utilized in combination with sand casting in order to take advantage of the design freedom provided by AM [32]. The 3D printed molds allow sensors to be embedded. This facilitates the collection of casting data from deep within molds. Using binder jetting, sand molds can be made with high compressive strength without the use of a pattern, which in turn can reduce cost and save on lead time [33]. Though patternless mold making presents a large time savings for RIC, the powder based AM processes it relies on need improvement. The main benefit of the patternless process is the ability to better incorporate metrology into the casting process [13]. It is clear that in order for solidification processes to benefit from unbounded design they must be coupled with AM.

2.3 Lattice Structures

AM processes have become increasingly relevant in different industries, especially in SLM of metals [34]. The current most prevalent application of SLM is manufacturing of lightweight cellular structures. The use of lattice structures is desirable because AM has allowed for the fabrication of topologies with

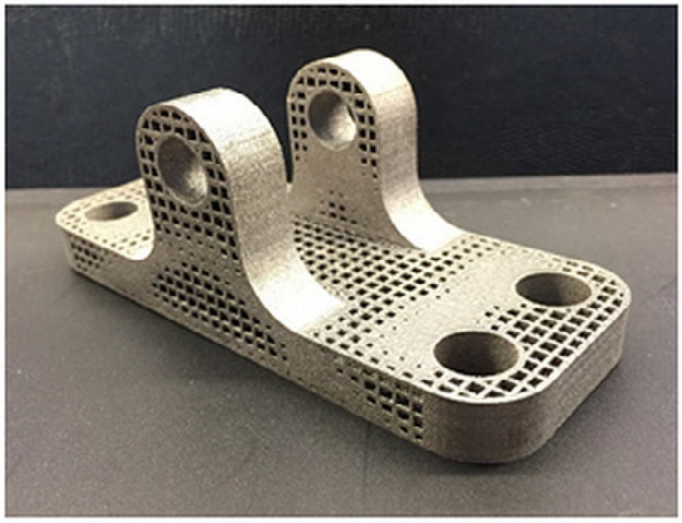

FIGURE 2.4: Optimized pillow bracket printed by EOS DMLS. Reprinted from [4] © 2019, with permission from Elsevier.

great geometrical complexity previously unachievable using traditional fabrication techniques [35]. Currently the only way to achieve components with very high specific stiffness or very high specific strength is using geometric methods like ordered porous lattice structures. Lattice structures can be used in lightweighting applications. Optimizing SLM manufacturing of lattices allows for better mechanical properties [36]. Lattice structures can be graded based on their SLM performance. One such example is a database evaluated by Tang et. al. [37]. Unlike SLM, an overarching analysis of the use of lattice structures in RIC is non existent. In some cases RIC could be better for cellular structures, using SLM, overprinting can be observed in the radius of the lattice truss. The truss overprinting is unpredictable [38]. This behaviour is less prevalent in RIC as the AM process is independent of the casting process. This makes the defects more predictable. This is just one of the few advantages of RIC for manufacturing of cellular structures. The two processes both have their pros and cons and their place in the metallic AM space.

Lattice structures can used to take advantage of the boundless design space provided by AM. Lattice structures can achieve controllable mechanical properties. This is done using ordered porous lattice structures [39, 40]. Lattice structures can even utilize programmable joints which result in lattices with

both stretch-dominated and bending-dominated behavior [41]. One application for controllable lattice structures is metallic bone design. The manufactured orthopaedic implants were found to be highly dependent on lattice geometry and relative density [42]. Lattice structures can be optimized by varying the unit cell topology, relative density, and base material. This optimization can be seen in Fig. 2.4. The authors designed an aero-bracket using a lattice structure topology optimization and manufactured using different types of AM processes. Beyond optimizing mechanical performance, lattice structures can be designed to be self-supporting [43]. Metal additive manufacturing (MAM) of complex parts with overhangs typically requires the use of sacrificial support structures to hold the part during the process [44]. The same is true for most AM processes. Support structures are essential for the good production of parts. Vaissier et al. presented a genetic-algorithm based framework for lattice support structure optimization [45]. Huang et al. utilized topology optimization to generate lattice support structures for maximizing heat conduction in SLM [46]. Beyond that lattice structures can be used for energy absorption. The AM of supportless lattice structures with TPU filaments and material extrusion processes such as FDM was evaluated for the application of energy absorption [47]. The authors found that supportless lattice structures inspired by sea urchin shells can improve the overall speed of the AM process for building customized parts. Lattice structures can be utilized for optimizing the self-supporting, heat conduction, energy absorption or lightweight performance of components. Although AM of lattice structures has been heavily researched, there is no existing study on lattice casting performance.

2.4 Applications of Rapid Investment Casting Lattice

According to Pattnaik et al. [48], IC has been used to manufacture: jewellery, art and weapons in ancient civilization. Given that IC can create parts with complex geometries, accurate dimensions and excellent surface finishes, it is no

surprise that fields such as: dental, biomedical and aerospace utilize this technology. Pattnaik et al. [49] stated that IC is superior to other casting practices and for this reason it can be applied to many applications such as: making automobile components, aircraft engines, jewelry, statues, prosthetics, computer hardware, electronics hardware, radar and machine tool components. With the unbounded design freedom provided by RIC and the isotropic nature of IC it can be used for many manufacturing applications requiring high accuracy. The following are some of the recent RIC advancements in the fields of biomedical engineering, dentistry and aerospace engineering.

IC as of late has showed a lot of promise for the manufacturing of implants in the biomedical field, given that components are generally individualized. Beyond that RIC is known for its ability to create complex 3D parts with excellent surface finishes which lends itself well to create lightweight components that don't lack in strength and interface well with the human body. Singh et al. [50] proposed the use of fused filament fabrication (FFF) for printing biomedical implants for use in IC. The study was focused on controlling surface roughness using three factors of the IC process such as slurry layers, slurry viscosity and dry time of primary layer. The research found that all three properties affected the surface quality of the cast hip joint and the research optimized the finish to micro-level resulting in a reduction of post processing operations. Singh et al. [51] later reviewed all the current research focused on improving the surface finish of FFF 3D printed patterns through parameter selection of IC and AM for biomedical implants. FFF is the AM method of choice for pattern making in the biomedical field due to its ability to create larger parts. One of the issues that remains to be resolved is the poor surface finish associated with FFF.

Dentistry has been using IC since 1897, Pattnaik et al. [48] stated that many dental laboratories employ the lost wax casting process. Given that every dentistry partial denture is unique to the anatomy of the patient, IC is perfect for this application. The conventional IC process has been replaced with RIC and instead of having crowns fit using molds, the process has been replaced by a

combination of 3D scanning,computer aided design/computer aided manufacturing (CAD/CAM) and RIC. A prime example of the use of IC in dentistry is Revilla-León and Özcan [52] who reviewed the different AM methods for processing the alloys used in dentistry. The authors compared SLM and direct metal laser sintering (DMLS) with casting. The results were that there are issues regarding accuracy and reproducibility with SLM and DMLS and for that reason there remains room for improvement in 3D printing metals. Alternatively Dahl et al. [53] investigated if single dental crowns designed using CAD and CAM would have as good a fit as those made with lost wax IC. Given the limited number of crowns tested, the authors were forced to reject the hypothesis that crowns made using CAD and CAM were similar to those produced using the conventional casting method. Given the unique geometry, high accuracy and surface finish requirements associated with dentistry, RIC is the manufacturing method of choice. The main struggle with the implementation of RIC in dentistry is the scanning and design aspect of the process rather than the casting process itself.

RIC can create parts with very little porosity, excellent surface finish and RIC parts can be used for applications where fatigue strength is critical. For this reason it is the obvious choice for manufacturing aerospace components. Wu et al [54] presented a new rapid casting process based on gelcasting and SLA. The process relies on the addition of an aqueous colloidal silica to the mold material slurry in order to rapidly cast hollow turbine blades. Given the need for accurate castings that aren't prone to creep, RIC is an ideal manufacturing method for turbine blades that have complex freeform surfaces and complex internal cooling channels, which can't be made using many other manufacturing processes. Wu et al. [55] later presented the use of the aforementioned gel casting technology for manufacturing turbine blades with film cooling holes. Compared to cylindrical cooling holes, abnormal cooling holes are more efficient. The new process was less time consuming and costly which in turn resulted in a higher production yield. Aguilar et al. [56] evaluated the use of IC to produce low pressure turbine blades made from intermetallic titanium aluminide alloys.

Given these blades are 50 percent lighter than the nickel-based alternative. The authors were able to qualify this production technology. In aerospace how much a component weighs is of great importance, being able to create components with more complex internal geometries instead of using assemblies can lead to significant weight savings and better performance. It seems that complex internal structures in aerospace have mostly been made using gelcasting, it would be interesting to further investigate the use of RIC for this process.

Chapter 3

Materials and Methods

This section outlines the parameters and setup used for the theoretical and experimental tests. The characterization methods and lattice structures used in the tests are also detailed.

3.1 Materials and Equipment

The AM machine used in this study is the 3D Systems FabPro 1000, a DLP printer with a resolution of 65 microns in the X and Y directions and 30-50 microns in the Z direction. The material used for this printer is the FabPro Proto GRY plastic resin. Proto GRY is a prototyping resin manufactured by 3D systems for prototyping. This resin was used due to its great printability when compared to casting resins. For this material, the Z direction can only achieve a resolution of 50 microns.

The casting machine used is the Neutec® J-2R™, and the flask is the 4" diameter and 6" tall Neutec® SuperPerf™ flanged flask. A high strength plaster – the Ransom and Randolph Ultra-Vest Maxx – is used as the mold material. The plaster is prepared with the CIMO St. Louis 92 - 4KG digital vacuum investment mixer. Heating of the mold is done in the Lucifer L17-K12 Furnace. Two casting materials are used in the experiments. One is the recycled 70-30 brass with a density of 8.73×10^3 g/mm^3, and the other one is the recycled 6061 aluminum with a density of 2.7×10^3 g/mm^3. The DenPlus Basic Eco Sandblaster is applied in post-processing, and the glass beads used in sandblasting have a size of 50 microns.

Samples are cut using a fret saw to perform grain structure analysis on the casts. Next, they get mounted in Bakelite using the Bueller SimpliMet 3000 compression press. The samples get lapped using 300, 400, 600, 800, and 1200 grit sandpapers. The samples get mirror-polished using alumina powder. Finally, they are etched using 200ml distilled water, 10gm Ferric chloride, and 50ml Hydrochloric acid. The void and grain structure analyses are done using the Keyence VHX-6000 microscope.

3.2 Manufacturing Process

The overall RIC process is illustrated in Fig. 3.1, and the necessary details are given in the following.

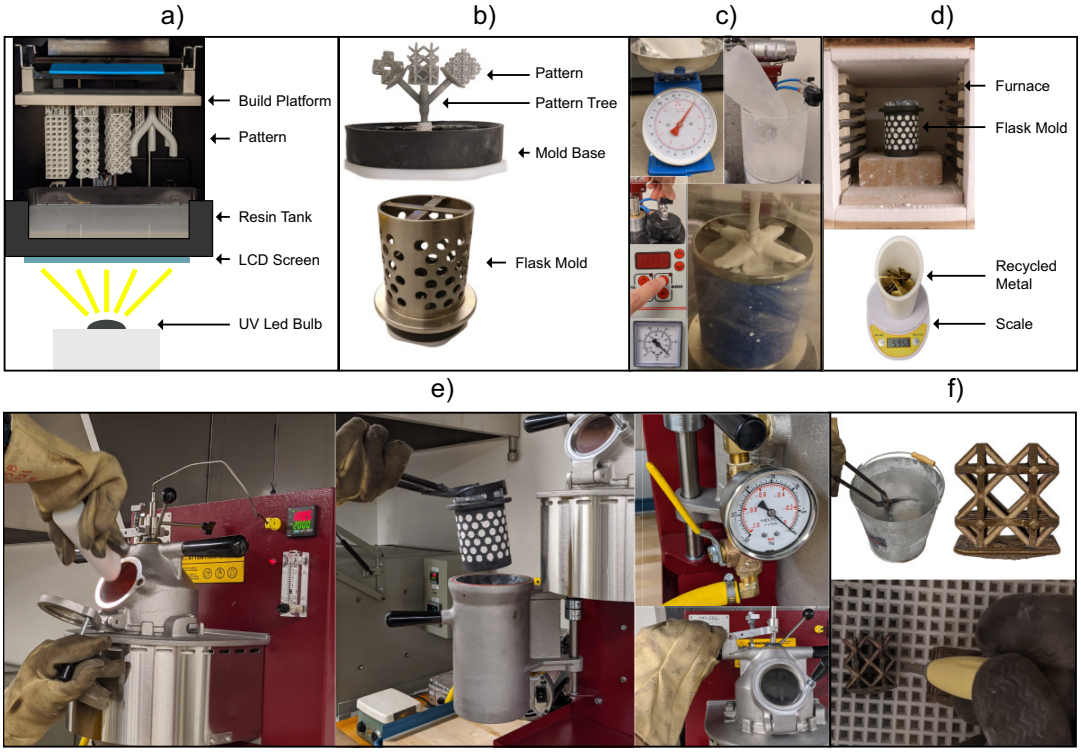

FIGURE 3.1: RIC process: a) DLP additive manufacturing. b) Pattern spruing. c) Plaster mold making. d) Pattern burnout. e) Vacuum casting. f) Post processing.

3.2.1 Pattern Making

A pattern has the shape of the object to be cast, so the computer-aided model (CAD) model is used to make the pattern. In RIC, the pattern is produced by

an AM machine, in this work the DLP printer is used (see Fig. 3.1(a)). After slicing the CAD model, DLP produces the pattern by using a projector to cure (solidify) complete layers of liquid resin at a time. The build head lowers into the resin tank, leaving one layer thickness between the head transparent and tank. The projector then exposes a mask of UV light through the transparent bottom of the tank. This mask is the two-dimensional (2D) profile of the current layer. After the layer curing, the tank tilts to detach the print from the build plate before moving up a layer thickness. This process repeats until the completion of the full 3D part. The main benefit of DLP is that it can create very high-quality patterns with great surface finishes [57]. Alternate AM processes that can be used for pattern making are MJM, SLA, and FFF see Fig. 1.1. DLP can achieve more complex overhangs using less supports thanks to it curing layer-by-layer instead of point-by-point and thus having better self-support capability of the material. Also, it is a lot faster than MJM and SLA while achieving a comparable resolution. FFF does not produce high enough quality parts for making delicate lattice structure patterns.

The same manufacturer offers a casting resin. The benefit of casting resin is that it creates less stress and ash in the mold during burnout. However, the casting resin was not rigid enough and did not print well. It also printed a lot slower than the prototyping resin, i.e., four times slower. Although the prototyping resin requires a higher temperature to be burnt out, it has significantly better printability, which was important as all the lattice topologies tested needed to be self-supporting to ensure there was no need for internal support removal.

3.2.2 Mold Making and Burnout

The printed pattern gets placed on a mold base and a steel flask is placed on top of the mold base. The perforated flask is then covered in masking tape to avoid spilling the plaster, see Fig. 3.1(b). The plaster then gets weighed based on the manufacturer's specifications and the volume of the flask and pattern. The plaster is placed in the mixer, and vacuum is pulled. Water is then added

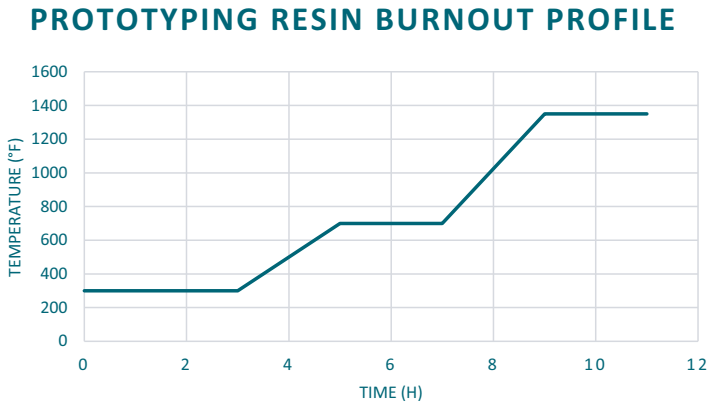

FIGURE 3.2: 3D Systems FabPro 1000 prototyping resin burnout profile

to the mixer based on the manufacturer's specifications, and the plaster gets hydrated 38%. The mixer then mixes the plaster for 7 minutes, at which point a knob is pulled to pour the plaster into the mold. Finally, the mold is vibrated to remove any bubbles from the plaster for another 7 minutes, see Fig. 3.1(c). The mold then gets removed from the mixer and is left for 10 minutes to dry. The mold containing the resin pattern then gets burnt out (Fig. 3.1(d)) with the custom burnout profile in Fig. 3.2.

3.2.3 Casting

For the casting experiment, the casting machine gets preheated to $1038°C$, and the mold gets preheated to $5388°C$. 150% weight of 70-30 brass was weighed and added to the casting machine's crucible for melting. The brass weight is calculated based on the density of 70-30 brass and the pattern volume. The reason of 150% mass was chosen is to ensure that there is an excess of metal, eliminating the lack of molten metal as a cause for casting defects. The recycled brass was melted down in the casting machine using argon shielding with a flow of 8L/min. Once the casting machine hit the melting temperature of $1038°C$, the recycled 70-30 brass was added to the machine, causing the machine's temperature to drop a few hundred $°C$. Once the temperature rose back to $1038°C$ and the metal was molten, the flask was introduced to the flask chamber. Vacuum was then pulled for the flask chamber before pulling the lever that

introduces the molten metal to the mold, see Fig. 3.1(e). The mold was then left under vacuum for 4 minutes to remove dissolved gases and fill the mold. After 4 minutes, the vacuum pump was turned off, and the mold was left to cool in the casting machine for 10 minutes. After 10 minutes the mold was removed from the machine and left to air cool. The cooling temperatures and times are optimal based on prior testing; these temperatures and time caused the least defects and stress cracking. Finally, once the mold had cooled to 200°C, the mold was quenched in a bucket of room temperature water.

For casting experiments involving 6061 aluminum, the whole process is basically the same. The only difference is that the casting machine preheat temperature is 649°C, and the mold preheat temperature is 315°C.

3.2.4 Post-processing

The majority of the plaster dissolves away from the quenching process. After quenching, the remaining plaster caught in small details gets sandblasted at 90 Psi, see Fig. 3.1(f). This removes minimal amounts of material without affecting geometric accuracy. Once all the plaster is removed from the sample, the feeder gets removed using a fret saw.

3.3 Lattice Designs

To test the casting performance of lattice structures, two sets of experiments with different designs are conducted. Two materials are used for the experiments as well to make sure it is the design rather than the material affecting the performance.

3.3.1 Set 1

In the first experiment, the set of lattice topologies includes rhombic, kelvin, cubic, and octet-truss, as shown in Fig. 3.3(a-d). These topologies were chosen as they are commonly used structures in AM, and they vary a lot in topology while remaining open celled and self-supporting. Each lattice unit cell is a

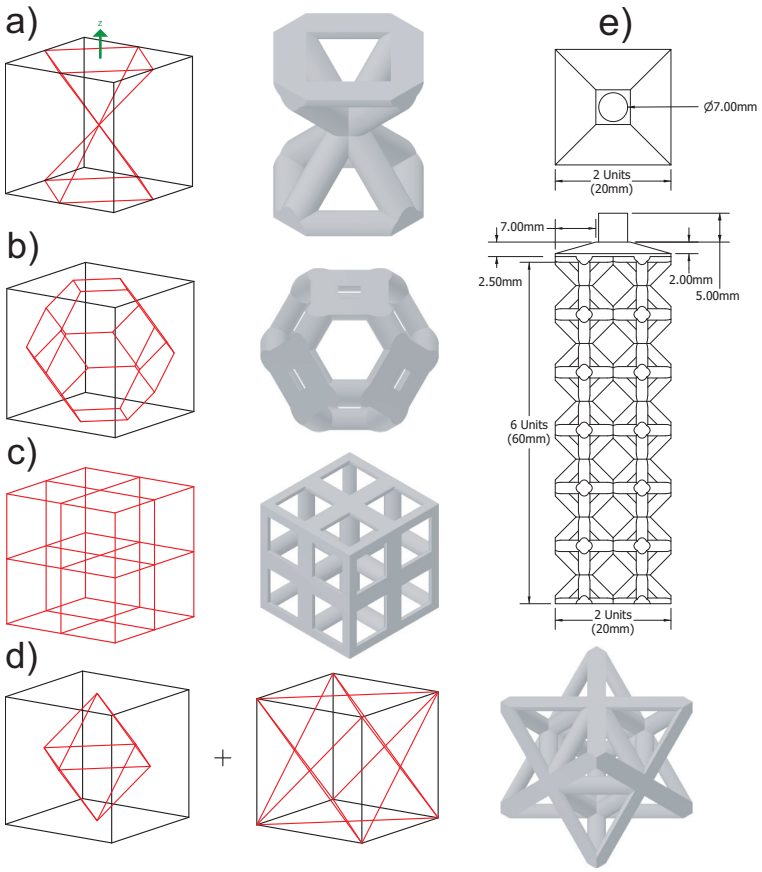

FIGURE 3.3: Test 1 lattice cells and structure: a) Rhombic. b) kelvin. c) Cubic. d) Octet-Truss. e) $2 \times 2 \times 6$ structure.

$10 \times 10 \times 10$ mm cube, and the green arrow on the wireframe cells is the Z-axis, which is the filling direction. Their connectivity are shown in order to better understand how they connect in 3D. All the topologies have a straight circular strut cross-section and a cubic packing strategy. The scope of topologies was narrowed in order to limit the amount of possible topologies. All four topologies have a constant volume and the strut size is changed to achieve this. The density of the unit cells is kept constant at 20%. The strut size needed to achieve a density of 20% for different lattice topologies were obtained through trial and error using Autodesk Inventor. The strut sizes for these topologies range from 1.3732 mm to 1.98020 mm. To better grade their filling performance and proneness to casting defects, the structures to be cast contain $2 \times 2 \times 6$ unit cells as shown in Fig. 3.3(e), and they were all fed via a 7 mm cylindrical feeder.

3.3.2 Set 2

For the second experiment, the main goal is to use the first experiment's observations to create lattice topologies more optimized for casting performance. Rhombic and octet-truss are being passed along from the previous experiment to serve as benchmarks compared to other publications and the previous experiment. Along with those two topologies, two more have been proposed. The four unit cells are rhombic, octet-truss, proposed cell, and hourglass. The structures, as well as their overall dimensions and orientation, can be seen in Fig. 3.4. The hourglass structure has a balance of vertical, horizontal, and 45° struts. This structure is used to evaluate further the effect of strut angle distribution on casting performance. The second proposed structure is one that was created purely for good casting performance. It has a low number of joints, low joint valence; most of its struts are 45°, and it has a large relative strut size. The hypothesis is that this combination of properties will lead to a better casting performance.

The unit cell size for this experiment is $5 \times 5 \times 5$ mm. This was chosen to observe more casting defects without exceeding the dimensions of the flask. In addition, the casting material was changed to 6061 aluminum. Due to the higher solidification shrinkage of aluminum compared to the brass, set 2 is a more challenging test beyond the geometry setting. This too will contribute to the ability to observe more casting defects to better grade the lattice topologies. The strut sizes for these samples ranged from 0.7 mm to 1.2 mm. This finer strut size will increase the likelihood of premature melt solidification which will more significantly differentiate the different topologies' performance. The structures to be cast contain $2 \times 2 \times 6$ unit cells as shown in Fig. 3.4(e) In order to feed the larger number of unit cells; the feeder size is being increased to 12 mm, which tapers from 15 mm. The 15 mm diameter was chosen to interface with the sprue base for the mold.

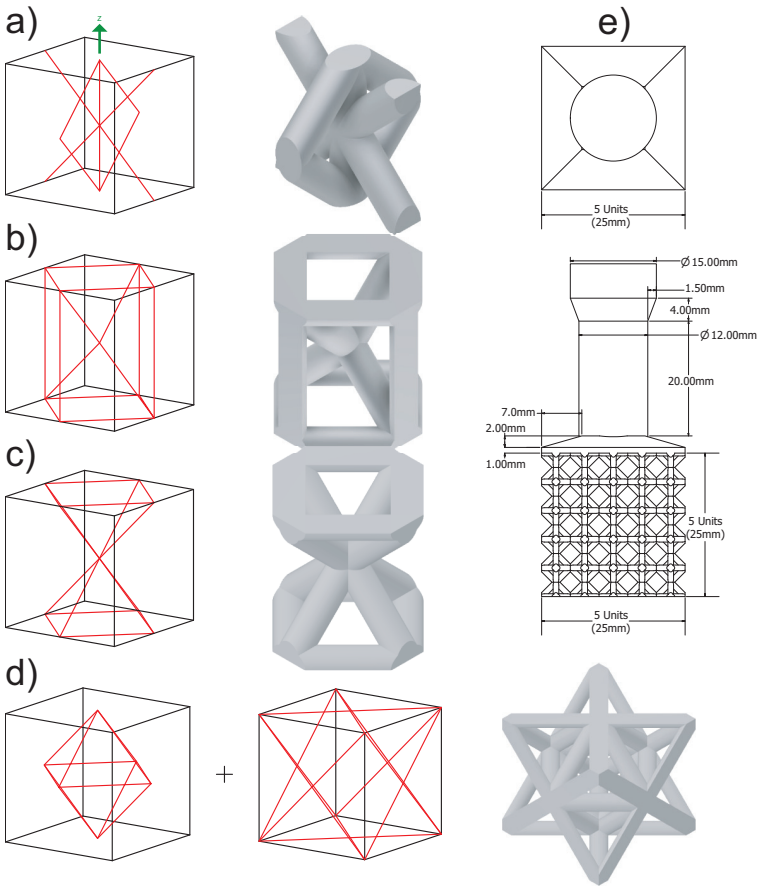

FIGURE 3.4: Test 2 lattice cells and structure: a) Proposed cell. b) Hourglass. c) Rhombic. d) Octet-Truss. e) $5 \times 5 \times 5$ structure.

3.4 Characterization

Analyses and characterizations based on both computer-aided engineering and physical experiments are conducted. They are detailed here.

3.4.1 Mold Flow Simulation

Mold flow simulations on various lattice structures were performed to grade the structures based on their casting performance. These simulations were performed in Altair Inspire Cast. The simulations were not used as exact representations of the different lattice structures' mold flow but were used as a comparison tool to see which samples performed better based on the following criteria: filling time, porosity, and cold shuts. Cold shuts refers to when multiple joining metal flows cool before properly fusing together.

The lattice structure geometry for the mold flow simulations is the same as the one to be cast in Fig. 3.3(e). Since the complexity of the second experimental structures was increased based on the results of the first. They were too complicated to simulate on a standard PC, and thus, this simulation was not conducted.

The mold flow simulation was performed using the parameters listed in Table 3.1. The simulation was a gravity process with the fill parameter set as a constant liquid level on the sprue. The casting method is IC, and a shell mold was chosen to simplify the simulation. The shell thickness of 50 mm is quite large and comparable to the casting experiments' flask mold. The 7 mm cylindrical feeder fed the molten metal as in Fig. 3.3(e). The elements utilized by the mold flow simulations are tetrahedral, and the software chose their size.

TABLE 3.1: Mold flow Altair Inspire Cast 2019.3 material properties

Property	**Value**	**Unit**
Material	CW502L Brass	N/A
Molding Material	Plaster	N/A
Melting Temp.	1093	$^{\circ}C$
Preheat Temp.	538	$^{\circ}C$
Shell Mold Thickness	50	mm

3.4.2 Mechanical Finite Element Analysis

Mechanical simulations were performed using Ansys Workbench 19.2. The material properties used for the simulations were 70-30 brass found in Table 3.2. Two static structural, mechanical simulations were performed per lattice sample: tension/compression and shear. Bending was omitted because if a lattice topology performed well under tension and compression, it also performed well under bending since bending is a combination of the two [58]. For the lattice topologies observed, the focus was lightweight, rigid topologies. Therefore the topologies were only loaded right up till the onset of plastic deformation. The results were only used to determine the equivalent tensile and shear modulus. Given that the only deformation observed was plastic and this Ansys simulation

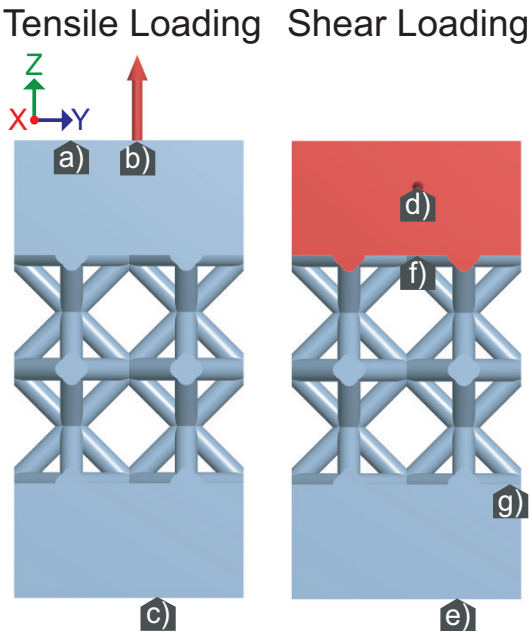

FIGURE 3.5: Loading conditions tensile: a) Displacement b) Force c) Fixed support. Loading conditions shear: d) Force e) Fixed support f) Displacement g) Displacement

did not take into account struts colliding with each other, the compressive simulations were the same as the tensile simulations, so they are not reported. Also, two large blocks of material were added to both ends of the lattice structure to ensure the loads are applied uniformly to the structure. For tensile loading, a force was applied to the top face 15 kN at a time. A fixed support was added to the bottom face, which restricts movement in every direction. Finally, a displacement constraint was added to the top face that only allows displacement in the direction of the applied load. For shear loading, a force was applied to the front face 15 kN at a time. A fixed support was also added to the bottom face, which restricts movement in every direction. Finally, a displacement constraint was added to both inner faces that only allowed displacement in the applied loading direction. The geometry for the mechanical tests was simplified as shown in Fig. 3.5, this was done to save on computation time. The purpose of the simulations was not to determine the exact deformation or maximum principal stress in the structures but rather to serve as a comparison tool for the different topologies to establish which ones have good cast-ability without sacrificing mechanical performance. The loading conditions and fixed supports

as well as the geometry utilized for the simulation, can be seen in Fig. 3.5. The observed results for mechanical performance are the max deformation in the applied load direction and the max principal stress. From these results, stress-strain graphs can be generated, and the resultant modulus for tensile and shear of the structure can be determined. These moduli will be used to compare the mechanical performance of the different lattice topologies.

TABLE 3.2: Ansys 70/30 [Cu/Zn] brass material properties

Property	**Value**	**Unit**
Density	8530	kg / m3
Young's Modulus	10E+10	Pa
Poisson's Ratio	.331	Pa
Bulk Modulus	8.08678E+10	Pa
Shear Modulus	3.080390E+10	Pa

3.4.3 Microscopic Analysis

A scaled-up lattice structure of the best performing lattice topology will be 3D printed, molded, and cast. The sample will then be cut into three smaller samples. The first sample will represent a joint of valence 2, the second one of four valence, and the last one six valence. Two sets of these six samples will be prepared. The samples will then be mounted in Bakelite, and their surfaces polished. The brass samples can then be etched and observed under the microscope for voids and grain structure analysis. Using the microscopic analysis images, each sample's void ratio can be determined, and the grain structure can be analyzed. The result should be an understanding of the effect that a lattice structure's joint valence has on the porosity and grain structure. The prediction is that that porosity will increase with joint valence. The struts will most likely exhibit a similar grain structure as most cast samples with a visible chill zone, columnar zone, and equiaxed zone.

Chapter 4

Results

4.1 Mold Flow

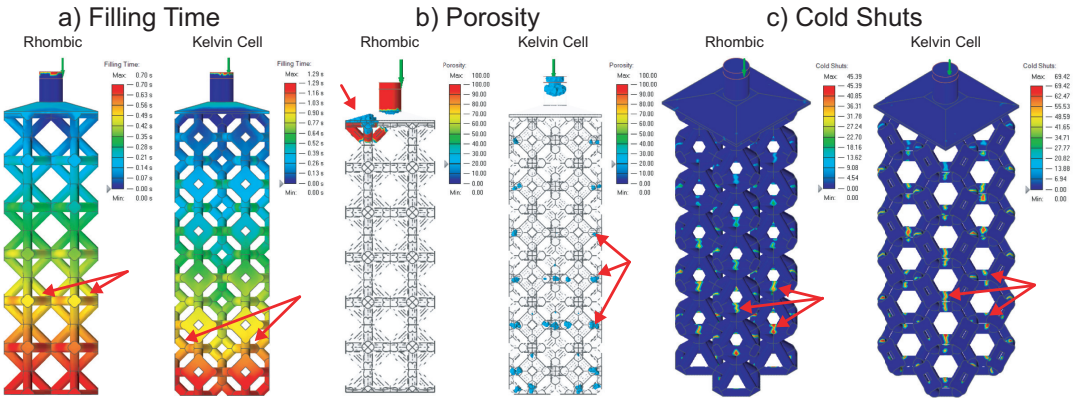

FIGURE 4.1: Flow simulation results for rhombic and kelvin

The results of the mold flow simulation can be seen in Fig. 4.1. The 3D plots of only the rhombic and kelvin structures are presented because both the cubic and octet-truss samples solidified before filling according to the simulation, so their results were not plotted. The three observed casting properties that showed the largest deviation across the lattice topologies were filling time, porosity, and cold shuts. Firstly, from the comparison of filling time, it can be seen that the rhombic structure fills fastest, and the filling time does not differ much in the x and y direction, only in the filling direction. Secondly, a porosity of 20% was chosen to be unacceptable and highlighted. The kelvin structure has repeatable porosity located at the horizontal struts (90° from filling direction). The rhombic structure shows almost no porosity of 20% in the body, but just at the top. This could be caused by the highly directional filling, which

would cause the feeder to solidify last. Finally, cold shuts were observed. The magnitude of cold shuts in the kelvin sample is higher than that of the rhombic sample. Cold shut locations for these two structures were consistently located on horizontal struts (90° from filling direction).

4.2 Cast 1

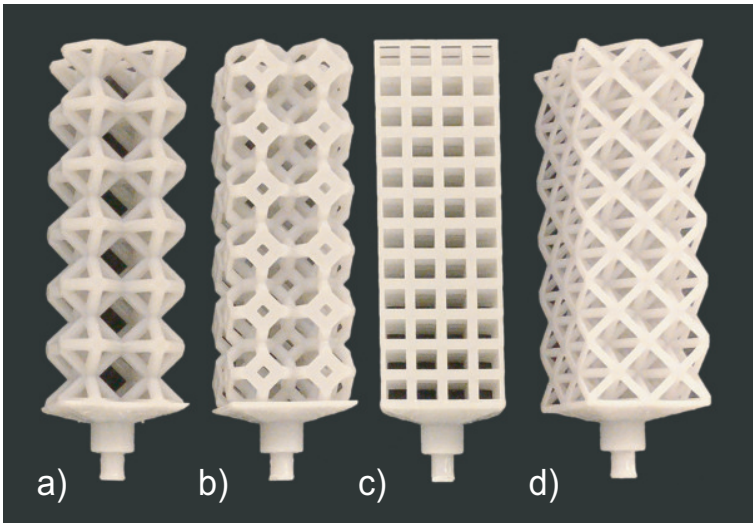

FIGURE 4.2: Printed Patterns Experiment 1 a) Rhombic b) kelvin c) Cubic d) Octet-Truss

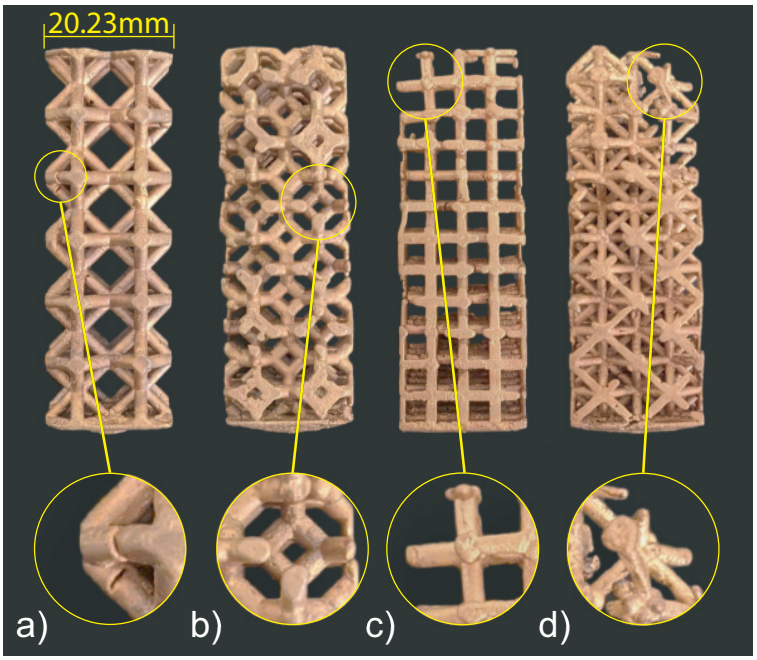

FIGURE 4.3: Set 1 cast structures: a) Rhombic, b) Kelvin, c) Cubic, and d) Octet-Truss.

TABLE 4.1: Lattice topology comparison casting experiment 1

Rhombic			
	Mass (g)	**Cell Width (mm)**	**Strut Diameter (mm)**
CAD	47.162	20.00	1.980
Printed	N/A	20.23	2.013
Cast	49.000	20.19	2.077
% Fill	**103.90**		
Kelvin			
	Mass (g)	**Cell Width (mm)**	**Strut Diameter (mm)**
CAD	47.163	20.00	1.976
Printed	N/A	20.21	2.090
Cast	45.840	20.15	2.047
% Fill	**97.19**		
Cubic			
	Mass (g)	**Cell Width (mm)**	**Strut Diameter (mm)**
CAD	47.142	20.00	1.629
Printed	N/A	20.20	1.723
Cast	40.350	20.15	1.693
% Fill	**85.59**		
Octet-Truss			
	Mass (g)	**Cell Width (mm)**	**Strut Diameter (mm)**
CAD	47.163	20.00	1.373
Printed	N/A	20.08	1.447
Cast	38.500	20.11	1.417
% Fill	**81.63**		

Following the presented manufacturing pipeline, all the lattice structures were successfully printed without supports, molded, and cast see Fig 4.2. Through visual inspection, the location and severity of casting defects can be observed. The octet truss and cubic structures did not fill, contrarily the rhombic and kelvin did. The kelvin has consistent defects on its horizontal struts (90° from filling direction) this was also visible in castings from other publications [59]. The rhombic structure also has defects on a few horizontal and diagonal struts, but this was not a consistent defect. Furthermore, the weights and dimensions of the CAD models, casts, and printed patterns are listed in Table 4.1. The measurements were taken using a caliper at three points on the structure's width and the struts. These three measurements get averaged, and they were taken randomly on the sample. For the width, any unfilled portions were avoided to make the measurements more accurate. Let it be noted that all the printed

lattice structures were around 1% larger in structure width than the CAD geometries. The biggest contributor to the inaccuracy in size seems to be caused by the 3D printing process, but this could be accounted for and corrected in the CAD models or the printer software. Because some samples are more filled than others, the measurements may not be a perfect representation as the unfilled samples will have a more significant variation in dimensions. The percent fill was calculated by comparing the cast part's mass from the CAD model to what it is. The percentage fill is based on the weight of the cast samples with the feeder removed compared to the CAD model's weight. According to the percent fill, the rhombic structure filled the most, followed by the kelvin, cubic and octet-truss. The percentage fill and visual inspection are in agreement. Overall the rhombic structure has the best casting performance. The structure seems to have flowed well based on the number of defects. The casting performance from best to worst was rhombic,

4.3 Cast 2

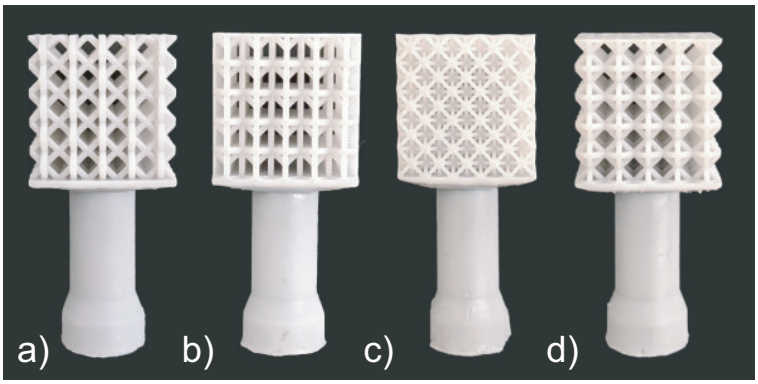

FIGURE 4.4: Printed Patterns Experiment 2: a) Proposed cell b) Hourglass c) Rhombic d) Octet-truss

All the four lattice structures in the second set are also successfully printed without supports, molded, and cast, as shown in Fig. 4.4 and Fig. 4.5. There was no significant variation in the samples' weight (see table 4.1). According to the percent fill, although the difference of the top-three was low, the most successful structure was the hourglass proceeded by the proposed cell, rhombic,

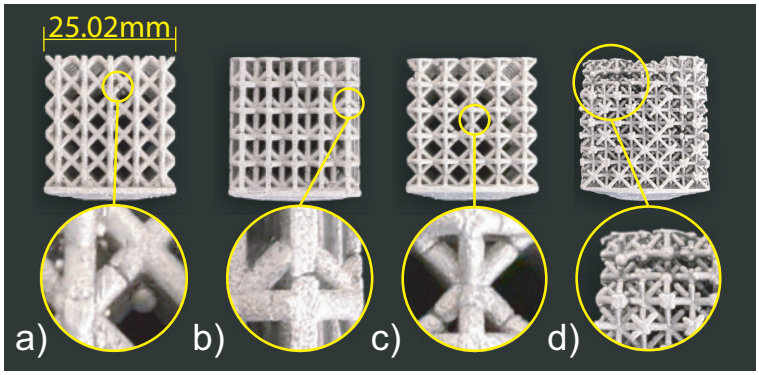

FIGURE 4.5: Set 2 cast structures: a) Proposed cell, b) Hourglass, c) Rhombic, and d) Octet-Truss.

and finally the octet-truss. However, from visual inspection, it is clear that the proposed cell structure showed the fewest visible defects, followed by the hourglass, rhombic, and finally octet-truss. The proposed cell sample only had one visibly unfilled strut. The hourglass sample had many visible defects present in its vertical (0° struts) as well as its joints among the vertical (0°), horizontal (90°) and diagonal (45°) struts. The rhombic structure had many defects similar to the first casting experiment with voids at the perpendicular (90°) struts and the high joint valence joints. Finally, the octet truss sample did not fill. From these results, it can be seen that the two new structures designed based on the observation from experiment 1 are indeed better.

4.4 Mechanical Properties

The tensile stress vs. strain for elastic deformation can be seen in Fig. 4.6. From the graph, it can be seen that under tensile loading, the hourglass, proposed cell and cubic samples performed the best. These three topologies had the highest resultant tensile modulus see Table 4.3. The resultant modulus of the structures describes the structures' rigidity under different loading conditions. The rigidity of the structures under tensile loading from highest to lowest is cubic, hourglass, proposed cell, rhombic, kelvin, and octet-truss. Similarly, the line's slope for shear stress against strain tells how much deformation occurs for a given applied shear load. The resultant shear modulus of the structures can be seen in Table 4.3. The structure's rigidity under shear loading from

Table 4.2: Lattice topology comparison casting experiment 2

Hourglass			
	Mass (g)	**Cell Width (mm)**	**Strut Diameter (mm)**
CAD	12.005	25.00	1.022
Printed	N/A	25.19	1.013
Cast	13.030	25.01	1.157
% Fill	**108.54**		
Proposed Cell			
	Mass (g)	**Cell Width (mm)**	**Strut Diameter (mm)**
CAD	12.004	25.00	1.111
Printed	N/A	25.02	1.147
Cast	12.750	24.93	1.113
% Fill	**106.21**		
Rhombic			
	Mass (g)	**Cell Width (mm)**	**Strut Diameter (mm)**
CAD	12.005	25.00	0.989
Printed	N/A	25.180	1.028
Cast	12.540	24.86	1.003
% Fill	**104.46**		
Octet-Truss			
	Mass (g)	**Cell Width (mm)**	**Strut Diameter (mm)**
CAD	12.005	25.00	0.686
Printed	N/A	25.10	0.743
Cast	11.740	20.080	1.447
% Fill	**97.79**		

highest to lowest is hourglass, proposed cell, octet-truss, rhombic, kelvin, and cubic. In terms of overall mechanical performance for shear and tensile, the hourglass structure performed the best closely followed by the proposed cell. The rhombic structure was the only other structure that performed well for both loading conditions. None of the other structures performed well for both loading conditions.

Table 4.3: Resultant modulus for simulated Ansys lattice structures. $\mathbf{E_{eq}}$ is the Equivalent Tensile Modulus and $\mathbf{G_{eq}}$ is the Equivalent Shear Modulus

Topology	$\mathbf{E_{eq}}$ **(Mpa)**	$\mathbf{G_{eq}}$ **(Mpa)**
Rhombic	14528	3387.3
kelvin	12849	2005.9
Cubic	24941	1214.8
Octet-Truss	11710	3478.2
Proposed Cell	23501	3978.4
Hourglass	24847	36225.0

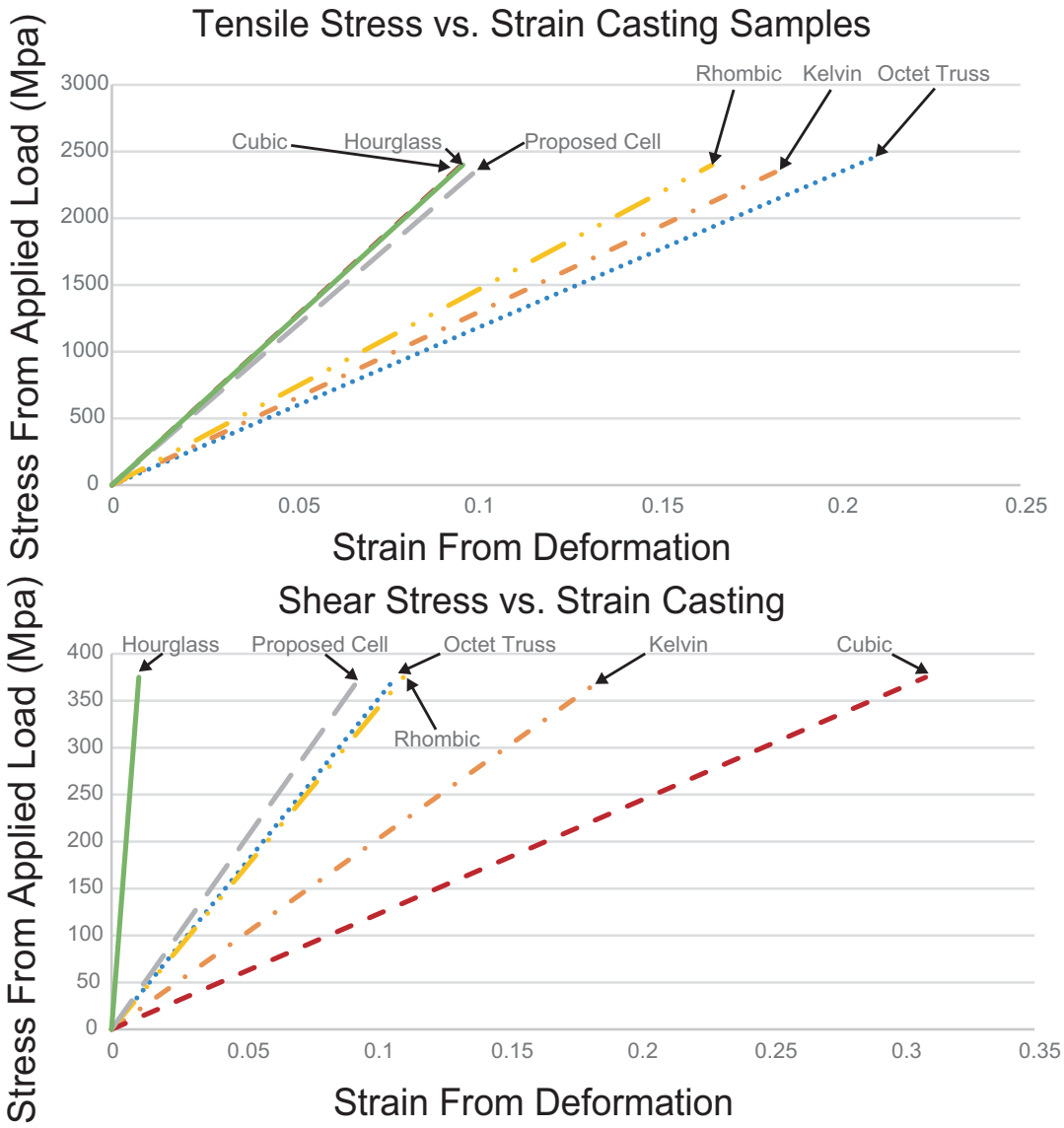

FIGURE 4.6: FEA results

4.5 Voids and Grain Structures

The proposed cell structure is cut on a plane containing 2-valence, 4-valence, and 6-valence joints. The results of the microscopic analysis can be broken down into two parts. The first is the analysis of resultant grain structure, and the second is the analysis of porosity in the cast samples. The resultant grain structure for the 2-valence, 4-valence, and 6-valence joints can be seen in Fig 4.8. The 2-valence and 4-valence joints both show clear indications of a chill, columnar, and equiaxed zone. The 6-valence joint seems to lack a fully formed equiaxed zone. This is most likely due to the cooling rate of this joint.

TABLE 4.4: Void properties. All area are in μm^2

Property	2-Valence	4-Valence	6-Valence
Sum of void area	28946	199025	786608
Max void area	1555	129721	82656
Min void area	20	20	20
Total void #	154	326	1209
Total strut area	13579304	13729209	23476110
Void ratio (%)	0.21	1.45	3.35

TABLE 4.5: Lattice topology strut size and joint characteristics. Strut size is in mm.

Property	Proposed	Hourglass	Rhombic	Cubic	Kelvin	Octet-Truss
Rel. Strut Size	0.22	0.20	0.20	0.16	0.20	0.14
Number of Joints	9	9	9	27	24	14
Max Joint Valence	6	6	8	6	4	16
Min Joint Valence	4	4	8	6	4	16
Mean Joint Valence	4.58	5.74	8	6	4	16

The grain area distribution was not determinable due to voids limiting the ability for software to determine the grain boundaries. The porosity results can be seen in Fig. 4.8, which shows the microscopic images at 50x magnification without having etched the sample. The area and frequency of each void were tabulated. The results for void ratio, number of voids, and max/min void area are summarized in Table 4.4. A clear trend from the results can be observed. With the increase in the joint valence, a higher void ratio is observed. The void ratio increases from 0.21% in the 2-valence joint to 1.45% in the 4-valence joint and finally to 3.35% in the 6-valence joint. The void ratio is based on the sum of the void area, so the void area shows the same trend. The number of defects also increases with the increase in joint valence. The only outlier in terms of behavior is the max void size. The max is higher for the 4-valence joint than the 6-valence joint. The large defect in the 4-valence joint is quite close to the strut's surface and could be a surface defect when looking at the structure as a whole. Regardless of this outlier, the overall void ratio still ends up being lower than the 6-valence one. These results show that the higher the valence number, the worse the casting performance.

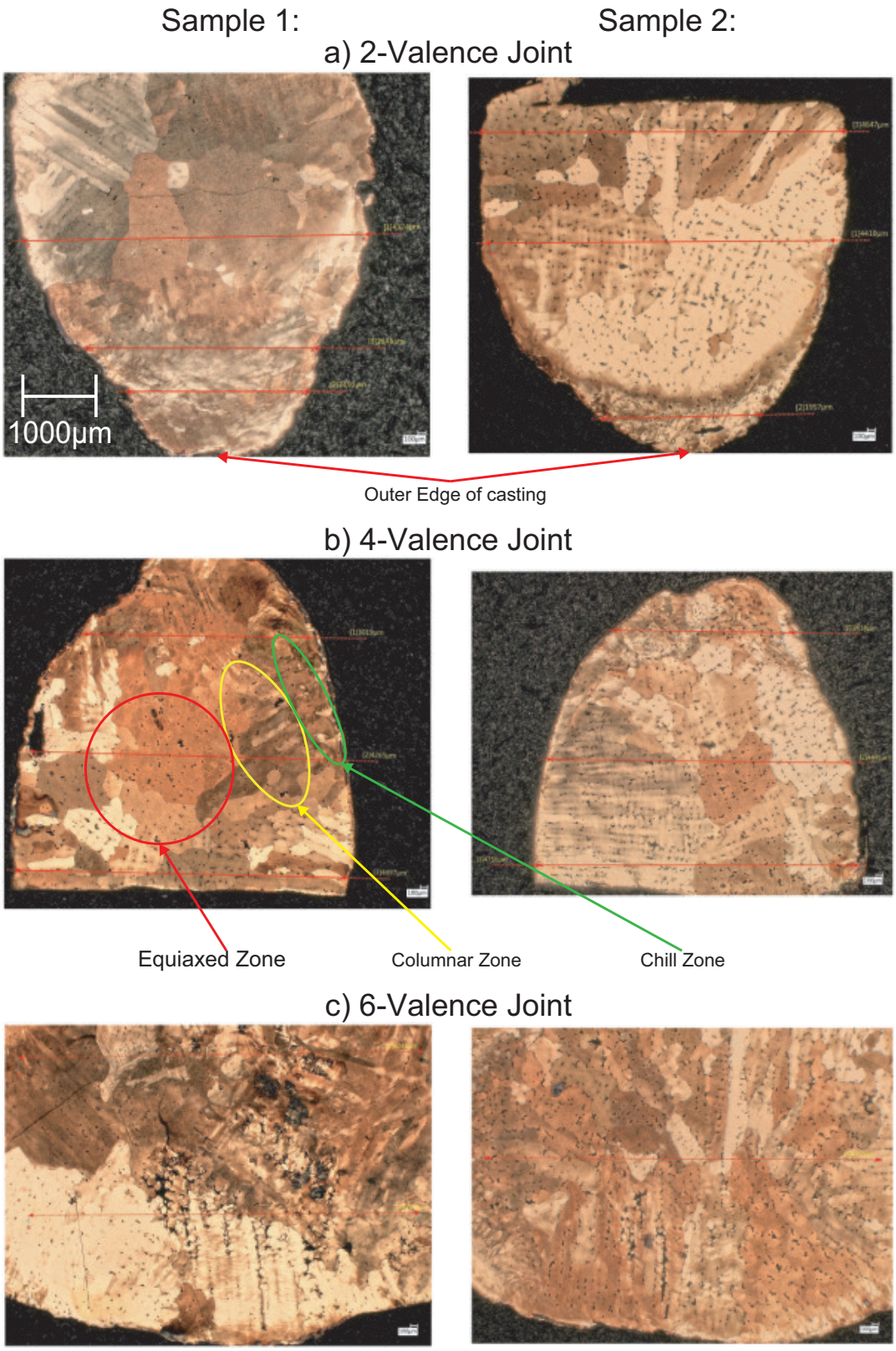

FIGURE 4.7: Microscopic analysis for grain structure. Images 50× magnification

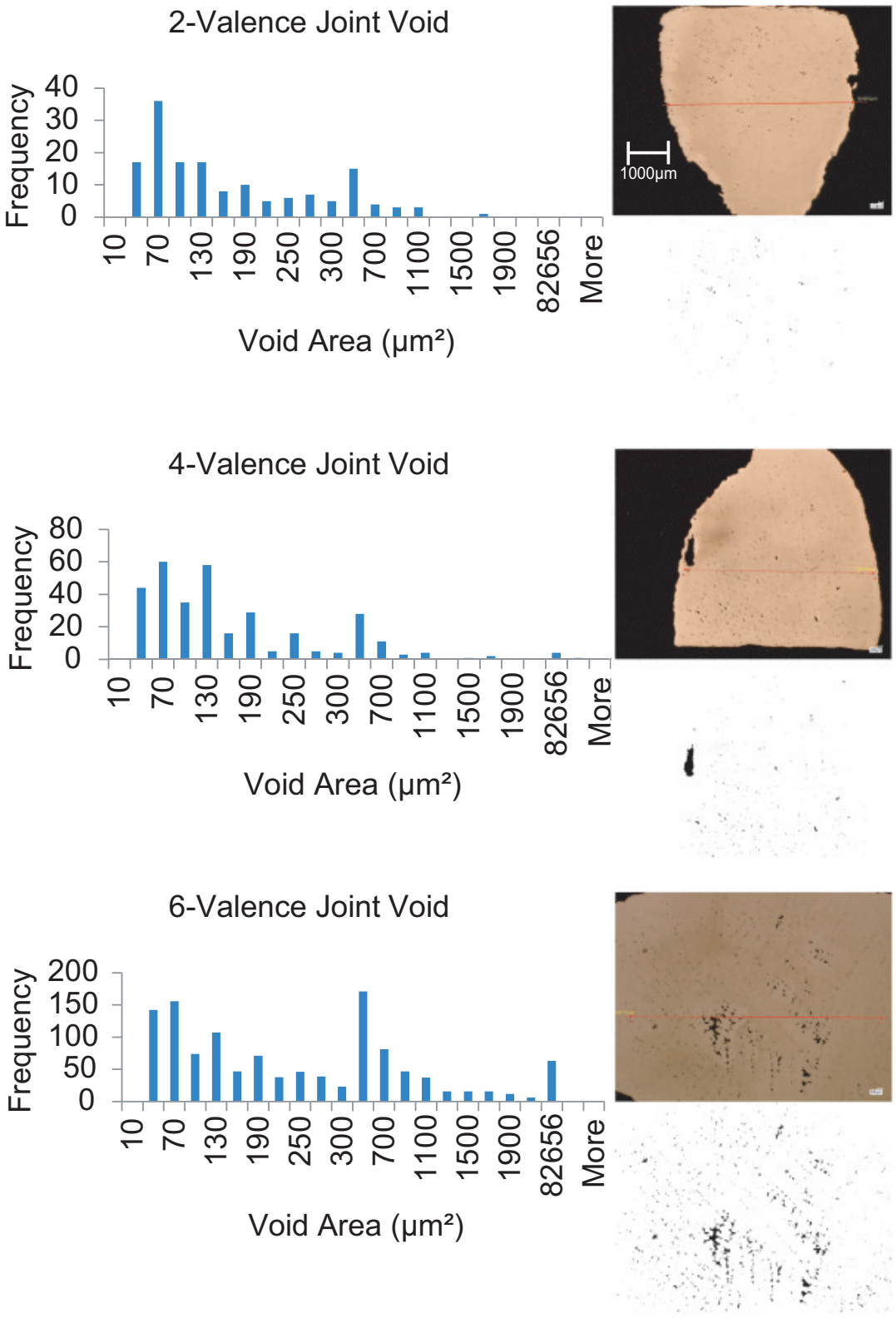

FIGURE 4.8: Microscopic analysis for porosity. Images 50× magnification

Chapter 5

Discussion

In terms of geometric accuracy, the printed lattice structures were larger in structure width than the CAD geometries, see table 4.1, and table 4.2. Some shrinkage was also observed in the cast part when compared to the printed pattern but this was less significant of a size change than the CAD geometry to the printed pattern. Overall the biggest contributor to the inaccuracy in final cast size seems to be caused by the 3D printing process but this could be accounted for and corrected in the 3D models or the printer software due to it being consistent.

From all the results, mold flow, the two casting experiments, and the FEA, The factors that significantly affect casting performance have been narrowed down. The properties that play a role in the success of the cast lattice topologies are: relative strut size, number of joints, joint valence, and strut angle distribution. The casting experiments' results and the overall performance of each lattice topology can be explained using these properties. The above properties are listed in Table. 4.5 for each lattice topology tested. Strut length is the distance traveled by the metal flow in the lattice cell. Strut length can be measured for different strut angles and divided by the total to determine the strut angle distribution (see Fig. 5.1).

When analysing the casting and mold flow results, the effect of relative strut size can be seen most significantly in the cubic and octet-truss topolgies. The two structures have lower relative strut sizes of 0.16 and 0.14 when compared to the more successful proposed cell and hourglass topologies (0.20-0.22) (see

Table 4.5). Lower relative strut sizes result in slower filling times which often results in premature melt solidification. Therefore, it is clear that the relative strut size plays the largest role in the success of a lattice structure casting. This ratio gives a idea of the negative effect that adding more struts for rigidity has on the strut size and in turn the metal flow. From this the structures that create an efficient short path for the metal to flow through can be determined.

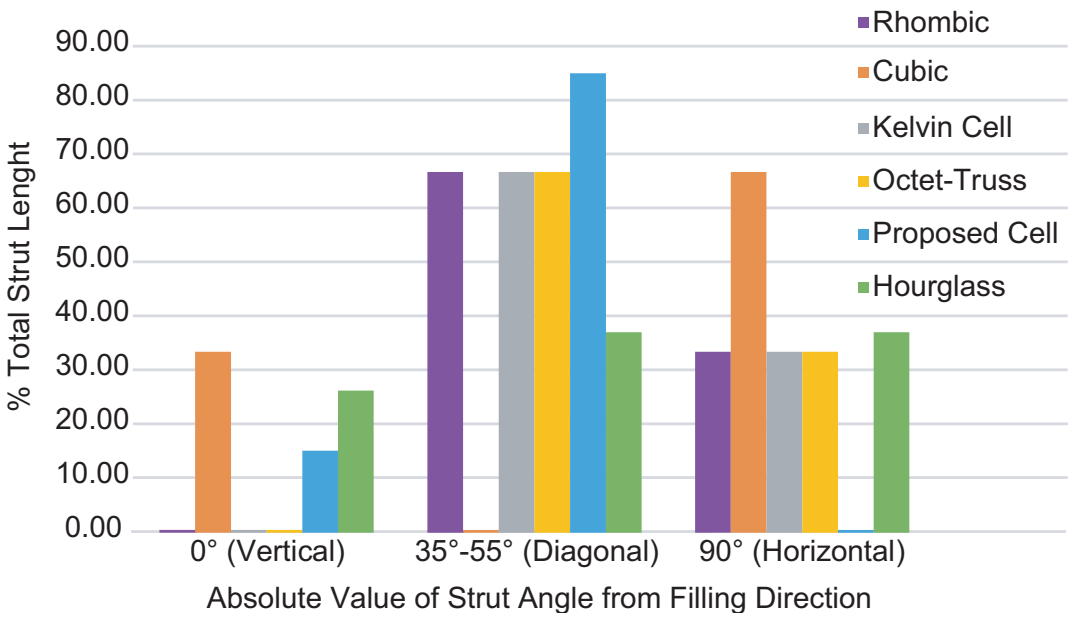

FIGURE 5.1: Topology strut angle distribution

Next in the level of importance is the number of joints. From the mold flow and experimental castings, it is clear that the topologies with the highest number of joints performed very poorly. The effect can be seen in the cubic (27), kelvin (24) and octet-truss (14) topologies. The remaining three topologies with a joint number of 9 all performed well. To add a level of granularity to the analysis, these three topologies can be further classified based on their joint valence. The proposed cell structure performed better than the other two due to its low joint valence (4.58), this trend continues for the hourglass (5.74) and then the rhombic (8). This behaviour can be further supported by the void analysis results. A higher void ratio can be observed as the joint valence is increased from 2 to 4 to 6. In the 2-valence and 4-valence joints, fully formed equiaxed zones can be seen unlike the 6-valence joint. Equiaxed grains are more

desirable as they exhibit better mechanical performance. The presence of the chill, columnar, and equiaxed zones are typical of cast or extruded parts due to the way they cool from the outside inward.

Finally, the effect of strut angle can definitely be seen in the casting results and the mold flow results, with defects often occurring at vertical or horizontal struts. Regardless, strut angle seems to have the smallest effect on the performance. The hourglass topology illustrates this as it was the second most performant but it has a balance of vertical, diagonal, and horizontal struts. This topology would have performed worse due to its horizontal and vertical struts if strut angle had more of an impact on the performance. From the FEA results, the presence of horizontal, diagonal, and vertical struts is important for mechanical strength under tensile and shear. Some of the structures were tested by Després et al. [58]. The authors observed similar behaviour as was observed in our FEA results. The diagonal struts contribute to the shear performance whereas the vertical struts contribute to the bending, tension and compression performance.

Overall looking at a balance of casting performance and mechanical strength, optimizing for relative strut size, number of joints, and joint valence seem to be the best way to avoid negatively affecting mechanical performance while improving casting performance. Mechanical performance can be achieved through strut angle distribution.

5.1 Design Guidelines

In order to better establish and understand the design guidelines for RIC, the performance grading of all the topologies can be seen in Table 5.1. The topologies are graded from 1 to 4 with 4 being the best and 1 being the worst performance. This table also includes the tensile and shear performance for reference.

The topological properties are listed in decreasing order of casting performance from left to right. The two topologies (proposed cell and hourglass) performed the best experimentally, as shown from the table. They scored 3 and

TABLE 5.1: Lattice topology performance grading (from 1 to 4.)

Property	Proposed	Hourglass	Rhombic	Kelvin	Cubic	Octet-Truss
Rel. Strut Size	4	4	3	3	2	1
Number of Joints	4	4	4	1	1	2
Joint Valence	3	3	3	4	3	1
Strut Angle Dist.	4	3	3	3	2	3
Tensile/Compressive	4	4	3	3	4	2
Shear	4	4	4	2	1	4

4 across the board and scored 4 in the most important categories (relative strut size, number of joints, and joint valence). The mechanical performance was not sacrificed due to the angle distribution, which includes vertical, horizontal, and diagonal struts [58].

The number of joints and joint valence also affect mechanical strength. This effect was observed in the FEA results and is supported by Li et al. [60]. The authors stated that lattice cells' deformation mode changes from bending-dominated to stretch-dominated with the increase of the joint valence. Stretch dominated is the more rigid of the two behaviors. Although, rigidity can be achieved without a high number of joints and joint valence, as Maxwell's criterion of rigidity is limited as demonstrated by Chen et al. [61]: if finite element analysis shows a rigid lattice, then the net lattice is rigid.

The design guidelines in order of importance are as follows. The relative strut size should be kept below 0.20. The number of joints should be kept below 9. The max and mean joint valence of 8 or less is recommended. Finally, for mechanical performance, the strut angle distribution should include vertical, diagonal, and horizontal struts. The following minimum conditions must be met for faithful use of the design guidelines.

- The lattice must be open celled, circular cross-sectioned, straight strut topologies with a cubic packing strategy.
- The lattice unit cell must range from 20 mm^3 to 1000 mm^3 and the strut size should range approximately from 1 mm to 5 mm.
- Lattice topologies should be oriented with the filling direction as demonstrated throughout the work.

- The materials cast should be similar in fluidity and solidification shrinkage to 70-30 brass or 6061 aluminum.
- The materials must be cast using some sort of assisted method such as vacuum or centrifugal with some sort of inert shielding gas.
- The pattern must be 3D printed using a resin or wax based process with a resolution of at least 100 μm in x, y and z.

By far from what has been tested, the proposed cell, hourglass and rhombic topologies meets all these criteria and achieve good casting and mechanical performance.

Chapter 6

Conclusion

In summary, it is clear that, much like other metallic AM processes, RIC can take full advantage of AM's unprecedented design freedom. RIC was successfully used to create a variety of lattice structures. These structures were utilized to determine the topological lattice properties critical to casting performance. From those results, a methodology to study the performance of RIC lattice structures has been established. In this methodology, topological properties are compared and analyzed using the test results. This analysis results in a set of design guidelines for RIC. The properties established to affect casting performance in descending importance are relative strut size, number of joints, joint valence, and strut angle distribution. These properties differ slightly but rely on the same logic as the design guidelines for casting. Feed paths and flow velocity/connectivity play a large role in design for casting. Without controlling these properties, hot spots, porosity and premature solidification can occur. All four proposed topological lattice properties directly affect a lattice's feed paths and flow velocity/connectivity. The design guidelines developed throughout this work differ in that they are specifically tailored towards optimizing cellular structures. Cellular structures by nature have a high potential for flow restriction or high connectivity. For this reason the design guidelines need to be more targeted than the general casting ones. The properties deemed to have the most significant effect on tensile and shear mechanical performance are strut angle distribution, number of joints, and joint valence. With the design methodology,

the proposed cell and hourglass topologies were created. These lattice topologies had the best overall casting and mechanical performance of all the tested lattices. The limitations of the current work include testing only strut-based lattice topologies. Future work could expand beyond this. Future work could also further refine the design methodology and automate the design process using software-driven methods.

Bibliography

[1] Fei Li, Yingchun Wang, Donghong Wang, Yanjie Zhao, Chengkang Qi, and Baode Sun. Comparison of various gating systems for investment casting of hydraulic retarder impeller with complex geometry. *Proceedings of the Institution of Mechanical Engineers, Part B: Journal of Engineering Manufacture*, page 0954405420971994, 2020.

[2] Jiangping Yu, Donghong Wang, Dayong Li, Ding Tang, Xin Hao, Shixin Tan, Da Shu, Yinghong Peng, and Baode Sun. Engineering computing and data-driven for gating system design in investment casting. *Int. J. Adv. Manuf. Technol.*, 111(3):829–837, 2020.

[3] Patrik Karlsson, Lars Pejryd, and Niclas Strömberg. Generative design optimization and characterization of triple periodic lattice structures in alsi10mg. In *International Conference on Additive Manufacturing in Products and Applications*, pages 3–16. Springer, 2020.

[4] Lin Cheng, Jiaxi Bai, and Albert C To. Functionally graded lattice structure topology optimization for the design of additive manufactured components with stress constraints. *Computer Methods in Applied Mechanics and Engineering*, 344:334–359, 2019.

[5] Nesma T Aboulkhair, Marco Simonelli, Luke Parry, Ian Ashcroft, Christopher Tuck, and Richard Hague. 3D printing of aluminium alloys: Additive manufacturing of aluminium alloys using selective laser melting. *Progress in Materials Science*, 106:100578, 2019.

[6] Tobias Maconachie, Martin Leary, Bill Lozanovski, Xuezhe Zhang, Ma Qian, Omar Faruque, and Milan Brandt. Slm lattice structures:

Properties, performance, applications and challenges. *Materials & Design*, 183:108137, 2019.

[7] S. Leuders, S. Meiners, L. Wu, A. Taube, T. Tröster, and T. Niendorf. Structural components manufactured by selective laser melting and investment casting—impact of the process route on the damage mechanism under cyclic loading. *J. Mater. Process. Technol.*, 248:130 – 142, 2017.

[8] C. Li, Z.Y. Liu, X.Y. Fang, and Y.B. Guo. Residual stress in metal additive manufacturing. *Procedia CIRP*, 71:348 – 353, 2018.

[9] V H Carneiro, S D Rawson, H Puga, J Meireles, and P J Withers. Additive manufacturing assisted investment casting: A low-cost method to fabricate periodic metallic cellular lattices. *Addit. Manuf*, page 101085, 2020.

[10] Yingjie Huang, Yingying Xue, Xinfu Wang, and Fusheng Han. Effect of cross sectional shape of struts on the mechanical properties of aluminum based pyramidal lattice structures. *Materials Letters*, 202:55–58, 2017.

[11] Hélder Puga, Vitor H Carneiro, P Correira, V Vieira, J Barbosa, and J Meireles. Mechanical behavior of honeycomb lattices manufactured by investment casting for scaffolding applications. *Proceedings of the Institution of Mechanical Engineers, Part L: Journal of Materials: Design and Applications*, 231(1-2):73–81, 2017.

[12] Nimesh A. Khirsariya, M. S. Kagthara, and P. H. Mandalia. Reduction of shrinkage defect in valve body casting using simulation software. *International Journal of Engineering Sciences & Research Technology*, 3(4):5021–5024, 2014.

[13] *Rapid Investment Casting: Design and Manufacturing Technologies*, volume Volume 1: 39th Computers and Information in Engineering Conference, 08 2019. V001T02A022.

[14] Jenn-Kun Kuo, Pei-Hsing Huang, Hsin-Yi Lai, and Jian-Rong Chen. Optimal gating system design for investment casting of 17-4PH stainless steel

enclosed impeller by numerical simulation and experimental verification. *Int. J. Adv. Manuf. Technol.*, 92(1-4):1093–1103, 2017.

[15] Donghong Wang, Jinyu Sun, Anping Dong, Da Shu, Guoliang Zhu, and Baode Sun. An optimization method of gating system for impeller by rsm and simulation in investment casting. *Int. J. Adv. Manuf. Technol.*, 98(9-12):3105–3114, 2018.

[16] Maidin S, T.M. Yi, Hambali A, Suriati Akmal, Ruzy Hambali, and Zulkeflee Abdullah. Investigation of optimum gating system design of fused deposition modelling pattern for sand casting. *J. Mechan. Eng. Sci.*, 11:2801–2814, 09 2017.

[17] P.-H. Huang and M.-J. Guo. A study on the investment casting of 17-4ph stainless steel helical impeller of centrifugal pump. *Mater. Res. Innov.*, 19(sup9):S9–77–S9–81, 2015.

[18] Marek Bruna, Dana Bolibruchová, Richard Pastirčák, and Anna Remišová. Gating system design optimization for investment casting process. *J. Mater. Eng. Perform.*, 28(7):3887–3893, 2019.

[19] Santosh Reddy Sama, Tony Badamo, Paul Lynch, and Guha Manogharan. Novel sprue designs in metal casting via 3D sand-printing. *Addit. Manuf*, 25:563–578, 2019.

[20] OMAR MOHD FAIZAN BIN MARWAH. *Analysis of various rapid prototyping techniques for investment casting.* PhD thesis, Universiti Teknologi Malay, 2016.

[21] Jiayi Wang, Santosh Reddy Sama, Paul Carl Lynch, and Guhaprasanna Manogharan. Design and topology optimization of 3D-printed wax patterns for rapid investment casting. *Procedia Manuf*, 34:683–694, 2019.

[22] Muslim Mukhtarkhanov, Asma Perveen, and Didier Talamona. Application of stereolithography based 3D printing technology in investment casting. *Micromachines*, 11(10):946, 2020.

[23] Jaspreet Singh, Rupinder Singh, and Harwinder Singh. Dimensional accuracy and surface finish of biomedical implant fabricated as rapid investment casting for small to medium quantity production. *J. Manuf. Process.*, 25:201–211, 2017.

[24] OMF Marwah, S Sharif, M Ibrahim, EJ Mohamad, and MH Idris. Direct rapid prototyping evaluation on multijet and fused deposition modeling patterns for investment casting. *Proceedings of the Institution of Mechanical Engineers, Part L: Journal of Materials: Design and Applications*, 230(5):949–958, 2016.

[25] Yoshiki Ishida and Taira Miyasaka. Dimensional accuracy of dental casting patterns created by 3d printers. *Dental materials journal*, 35(2):250–256, 2016.

[26] Mario Monzon, Zaida Ortega, Alba Hernandez, Ruben Paz, and Fernando Ortega. Anisotropy of photopolymer parts made by digital light processing. *Materials*, 10(1), 2017.

[27] Pei-Hsing Huang and Wei-Ju Huang. Processing design of miniature casting incorporating stereolithography technologies. *International Journal of Mechanical, Aerospace, Industrial, Mechatronic and Manufacturing Engineering*, 11(8):1403 – 1406, 2017.

[28] Parlad Kumar, Inderpreet S. Ahuja, and Rupinder Singh. Effect of process parameters on surface roughness of hybrid investment casting. *Progress in Additive Manufacturing*, 1(1):45–53, Jun 2016.

[29] MN Hafsa, N Kassim, S Ismail, SA Kamaruddin, TM Hafeez, Batu Pahat, M Ibrahim, and ZH Samsudin. Study on surface roughness quality of fdm and mjm additive manufacturing model for implementation as investment casting sacrificial pattern. *Journal of Mechanical Engineering*, 2018.

[30] Mustaffa Ibrahim and MN Hafsa. Dimensional accuracy of additive manufacturing model with different internal structure for investment casting implementation. *International Integrated Engineering Summit (IIES 2014)*, 2014.

[31] Munish Chhabra and Rupinder Singh. Experimental investigation of pattern-less casting solution using additive manufacturing technique. *MIT International Journal of Mechanical Engineering*, 1(1):17–25, 2011.

[32] Jason Walker, Evan Harris, Charles Lynagh, Andrea Beck, Rich Lonardo, Brian Vuksanovich, Jerry Thiel, Kirk Rogers, Brett Conner, and Eric MacDonald. 3d printed smart molds for sand casting. *Int. J. Metalcast.*, 12(4):785–796, 2018.

[33] Yashkumar Patel, Ankit Kahar, and Dhaval Doshi. Technical Review of Additive Manufacturing technique in Patternless Casting Manufacturing. *Int J S Res Sci. Tech.*, page 6, 2018.

[34] Amir M Aboutaleb, Mohammad J Mahtabi, Mark A Tschopp, and Linkan Bian. Multi-objective accelerated process optimization of mechanical properties in laser-based additive manufacturing: Case study on selective laser melting (slm) ti-6al-4v. *Journal of Manufacturing Processes*, 38:432–444, 2019.

[35] Oraib Al-Ketan, Reza Rowshan, and Rashid K Abu Al-Rub. Topology-mechanical property relationship of 3D printed strut, skeletal, and sheet based periodic metallic cellular materials. *Addit. Manuf.*, 19:167–183, 2018.

[36] Zhen Wang, Zhiyu Xiao, Ying Tse, Chuanshou Huang, and Weiwen Zhang. Optimization of processing parameters and establishment of a relationship between microstructure and mechanical properties of slm titanium alloy. *Optics & Laser Technology*, 112:159–167, 2019.

[37] Li Tang, Qingbiao Zhang, Keshan Liang, Xiqing Zhao, and Zhixiong Zhang. Discrete optimization of internal part structure via slm unit structure-performance database. *Metals*, 8(1):45, 2018.

[38] Lina Yan, Li Ping Zhao, and Gavin Kane O'Neill. Dimensional consistency of SLM printed orthopaedic implants designed using lightweight structures. *Transactions on Additive Manufacturing Meets Medicine*, 2(1), 2020.

[39] Han Wang, Yu Fu, Mingming Su, and Hai Hao. A novel method of indirect rapid prototyping to fabricate the ordered porous aluminum with controllable dimension variation and their properties. *Journal of Materials Processing Technology*, 266:373–380, 2019.

[40] Dawei Li, Wenhe Liao, Ning Dai, Guoying Dong, Yunlong Tang, and Yi Min Xie. Optimal design and modeling of gyroid-based functionally graded cellular structures for additive manufacturing. *Comput. Aided Des.*, 104:87–99, 2018.

[41] Marius A Wagner, Thomas S Lumpe, Tian Chen, and Kristina Shea. Programmable, active lattice structures: Unifying stretch-dominated and bending-dominated topologies. *Extreme Mechanics Letters*, 29:100461, 2019.

[42] Enrique Alabort, Daniel Barba, and Roger C Reed. Design of metallic bone by additive manufacturing. *Scripta Materialia*, 164:110–114, 2019.

[43] Ajeet Kumar, Luca Collini, Alix Daurel, and Jeng-Ywan Jeng. Design and additive manufacturing of closed cells from supportless lattice structure. *Additive Manufacturing*, page 101168, 2020.

[44] Ahmed Hussein, Liang Hao, Chunze Yan, Richard Everson, and Philippe Young. Advanced lattice support structures for metal additive manufacturing. *Journal of Materials Processing Technology*, 213(7):1019–1026, 2013.

[45] Benjamin Vaissier, Jean-Philippe Pernot, Laurent Chougrani, and Philippe Véron. Genetic-algorithm based framework for lattice support structure

optimization in additive manufacturing. *Computer-Aided Design*, 110:11–23, 2019.

[46] Renkai Huang, Ning Dai, Xiaosheng Cheng, and Lei Wang. Topology optimization of lattice support structures for heat conduction in selective laser melting. *The International Journal of Advanced Manufacturing Technology*, 109(7):1841–1851, 2020.

[47] Ajeet Kumar, Saurav Verma, and Jeng-Ywan Jeng. Supportless lattice structures for energy absorption fabricated by fused deposition modeling. *3D Printing and Additive Manufacturing*, 7(2):85–96, 2020.

[48] Sarojrani Pattnaik, D Benny Karunakar, and PK Jha. Developments in investment casting process—a review. *Journal of Materials Processing Technology*, 212(11):2332–2348, 2012.

[49] Sarojrani Pattnaik, Pradeep Kumar Jha, and D Benny Karunakar. A review of rapid prototyping integrated investment casting processes. *Proc. Inst. Mech. Eng. Pt. L J. Mater. Des. Appl.*, 228(4):249–277, 2014.

[50] Rupinder Singh, Sunpreet Singh, and Prince Kapoor. Investigating the surface roughness of implant prepared by combining fused deposition modeling and investment casting. *Proceedings of the Institution of Mechanical Engineers, Part E: Journal of Process Mechanical Engineering*, 230(5):403–410, 2016.

[51] Daljinder Singh, Rupinder Singh, and Kamaljit Singh Boparai. Development and surface improvement of fdm pattern based investment casting of biomedical implants: A state of art review. *J. Manuf. Process.*, 31:80 – 95, 2018.

[52] Marta Revilla-León and Mutlu Özcan. Additive manufacturing technologies used for 3d metal printing in dentistry. *Current Oral Health Reports*, 4(3):201–208, Sep 2017.

[53] Bjorn Einar Dahl, Hans Jacob Ronold, and Jon E. Dahl. Internal fit of single crowns produced by cad-cam and lost-wax metal casting technique assessed by the triple-scan protocol. *The Journal of Prosthetic Dentistry*, 117(3):400 – 404, 2017.

[54] H Wu, D Li, Y Tang, N Guo, F Cui, and B Sun. Rapid casting of hollow turbine blades using integral ceramic moulds. *Proc. Inst. Mech. Eng. B. J. Eng. Manuf.*, 223(6):695–702, 2009.

[55] Haihua Wu, Dichen Li, Xiaojie Chen, Bo Sun, and Dongyang Xu. Rapid casting of turbine blades with abnormal film cooling holes using integral ceramic casting molds. *Int. J. Adv. Manuf. Technol.*, 50(1-4):13–19, 2010.

[56] Julio Aguilar, Andre Schievenbusch, and Oliver Kättlitz. Investment casting technology for production of tial low pressure turbine blades – process engineering and parameter analysis. *Intermetallics*, 19(6):757 – 761, 2011.

[57] C.-D. Matte, M. Pearson, F. Trottier-Cournoyer, A. Dafoe, and T. H. Kwok. Automated storage and active cleaning for multi-material digital-light-processing printer. *Rapid Prototyping J.*, 25(5):864 – 874, 2019.

[58] Nathaniel Després, Edward Cyr, and Mohsen Mohammadi. A performance metric for additively manufactured microlattice structures under different loading conditions. *Proceedings of the Institution of Mechanical Engineers, Part L: Journal of Materials: Design and Applications*, 233(9):1814–1829, 2019.

[59] Yanpeng Wei, Bo Yu, Quanzhan Yang, Peng Gao, Zhiquan Miao, Jingchang Cheng, and Xun Sun. Damping behaviors of steel-based kelvin lattice structures fabricated by indirect additive manufacture combining investment casting. *Smart Materials and Structures*, 29(5):055001, 2020.

[60] Chuanlei Li, Hongshuai Lei, Zhong Zhang, Xiaoyu Zhang, Hao Zhou, Panding Wang, and Daining Fang. Architecture design of periodic truss-lattice cells for additive manufacturing. *Addit. Manuf*, page 101172, 2020.

[61] Wen Chen, Seth Watts, Julie A Jackson, William L Smith, Daniel A Tortorelli, and Christopher M Spadaccini. Stiff isotropic lattices beyond the maxwell criterion. *Science advances*, 5(9), 2019.